Multiscale 'whole-cell' models to study neural information processing – new insights from fly photoreceptor studies

Zhuoyi Song[1,2*], Yu Zhou[3], Jianfeng Feng[2], Mikko Juusola[4,5*]

[1]MOE Frontiers Center for Brain Science, Institute of Science and Technology for Brain-inspired Intelligence, Fudan University, Shanghai 200433, China
[2]Key Laboratory of Computational Neuroscience and Brain-Inspired Intelligence (Fudan University), Ministry of Education, China
[3]School of Computing, Engineering and Physical Sciences, University of Central Lancashire, Preston PR1 2HE, UK
[4]Department of Biomedical Science, University of Sheffield, Sheffield S10 2TN, UK
[5]State Key Laboratory of Cognitive Neuroscience and Learning, Beijing Normal University, Beijing 100875, China

* Correspondence: songzhuoyi@fudan.edu.cn or m.juusola@sheffield.ac.uk

3-5 highlights

- The first dynamic neuron "whole-cell" neuron models, built for fly photoreceptors.

- Neural information processing at the mechanistic, algorithmic and the computational levels.

- Explanations why sensory neuron process structured stimuli better than Gaussian white noise

- Subcellular refractory period and stochastic sampling greatly benefit encoding in graded potential systems.

- Photoreceptor microsaccades sharpen retinal images of moving objects, enabling hyperacute vision.

Abstract

Understanding a neuron's input-output relationship is a longstanding challenge. Arguably, these signalling dynamics can be better understood if studied at three levels of analysis: computational, algorithmic and implementational (Marr, 1982). But it is difficult to integrate such analyses into a single platform that can realistically simulate neural information processing. Multiscale dynamical "whole-cell" modelling, a recent systems biology approach, makes this possible. Dynamical "whole-cell" models are computational models that aim to account for the integrated function of numerous genes or molecules to behave like virtual cells *in silico*. However, because constructing such models is laborious, only a couple of examples have emerged since the first one, built for *Mycoplasma genitalium* bacterium, was reported in 2012. Here, we review dynamic "whole-cell" neuron models for fly photoreceptors and how these have been used to study neural information processing. Specifically, we review how the models have helped uncover the mechanisms and evolutionary rules of quantal light information sampling and integration, which underlie light adaptation and further improve our understanding of insect vision.

Keywords: "whole-cell" modelling; neural information processing; insect vision; fly photoreceptor

Introduction

Single neurons are the main building blocks of the nervous system. A central problem in neuroscience is to understand mechanistically how neurons sample and communicate information. Quantitative computational models can help reproduce a neuron's physical properties, simulate its dynamics, and approximate its information processing. However, incorporating the essential details to achieve

appropriate model complexity with computational tractability is a notoriously difficult balancing act (Herz et al., 2006). As Yakov Frenkel (1894–1952), a Russian physicist, mulled: *A good theoretical model of a complex system should be like a good caricature: it should emphasise those features, which are most important and should downplay the inessential details. However, the only snag with this advice is that one does not really know which are the inessential details until one has understood the phenomena under study* (Hemberger et al., 2016). To search for the essential details to study neural information processing, we think there is a need for biomimetic "whole-cell" neurons models, which implement microscopic molecular details to reproduce macroscopic cellular input-output dynamics. We will next highlight this point by briefly reviewing the major single-neuron model categories.

A brief overview of single-neuron model categories in computational neuroscience

Single-neuron models fall into two major categories: detailed biophysical models and simple phenomenological models. The phenomenological models adopt a reductionist approach, aiming to derive the simplest mathematical format describing a particular feature of a stimulus-response function. Such models can be derived from experimental data or can emerge from theoretical derivations out of first principles. The models typically start from empirical mathematical descriptions, such as Volterra filter series and static nonlinearities (French et al., 1993; Juusola et al., 1995b), with parameters fitted to reproduce neural responses to explicit stimuli (Ostojic and Brunel, 2011). However, because these generic black-box "block-components" are too simple to mimic real neurons' adaptive sampling dynamics, the models provide limited predictive power and generalisability beyond the tested conditions and cannot respond like real neurons to a broad range of stimuli (Juusola et al., 2017; van Kleef et al., 2010).

To study how the emergent properties come about from complex systems, such as living cells, it seems reasonable to construct bottom-up biomimetic models, which aim to replicate the cell's ultrastructure, signalling pathways and response dynamics. Such biologically-realistic models follow a constructionist approach, assembling the relevant biological details to achieve sufficient verisimilitude for the neuron's workings to be studied systematically and understood mechanically (Clark et al., 2013; Juusola et al., 2017).

Whilst there is a spectrum of neuronal modelling techniques that lie between the phenomenological and biologically-realistic models (Herz et al., 2006), we focus on the most detail-oriented single neuron models because they can act as diagnostic simulation platforms to understand the studied phenomena. Trendsettingly, these modelling approaches are being applied in large regional brain initiatives, such as the human brain project (HBP), highlighting their growing influence on the field.

The HBP hypothesises that building biologically accurate brain models can help explore the emergence of biological intelligence (Markram, 2006). The "realistic" single neuron models have shown their emergent explanatory power in revealing the mechanisms for a neuron's nonlinear signalling dynamics, with examples tabled in (Herz et al., 2006). It is even assumed that these kinds of complex single-neuron computations may underlie biological intelligence. For example, Goriounova et al. showed *in silico*, with a detailed pyramidal neuron model, that more extensive and more complex dendrites of human pyramidal neurons may associate with large temporal cortical thickness and high IQ scores, reflecting fast action potential kinetics (Goriounova et al., 2018).

More than a decade ago, scientists began to use the biologically-detailed single neuron models to simulate large neuronal population activity (Markram, 2006, 2012; Markram et al., 2015). The Blue Brain Project, a collaboration between EPFL and the IBM computing corporation, even started to assemble 100,000 "realistic" neuron models to simulate a rat's neocortical column, considered to be an elementary cortical unit within the brain (Markram, 2006, 2012; Markram et al., 2015). More recently, biological-realistic simulation of large neural networks is included in several well-funded national and global brain initiatives, including the Human Brain Project (HBP) (Markram, 2012) and Obama's BRAIN initiatives (Szalavitz, 2013). The on-going China Brain Project (Poo et al., 2016) also emphasises a more applied aspect, the brain-inspired Artificial Intelligence (AI). However, we would like to take a step back and look critically at this "realistic" neuronal modelling approach, asking: "is the current realistic neuronal modelling approach realistic?".

2

Biophysical single neuron models originate from the Hodgkin-Huxley's formalism (Hodgkin and Huxley, 1952), which simulates how action potentials arise from two specific ion-channel population's push-pull dynamics on the cell membrane. Wilfred Rall recognised that the complexity of the dendritic and axonal structures would profoundly affect a neuron's voltage generation and propagation (Rall, 1959) and developed the cable theory to quantify how current flows in realistic neuronal structures (Rall, 1964). The main idea was to segment the neurons into many little compartments, following their real morphology, building HH models for each compartment, and connecting them by resistors through which axial current flows. Such detailed compartmental models are currently the most widely-used biologically "realistic" neuronal models. They can be quite complicated, with a single model composed of tens of thousands of compartments (Goriounova et al., 2018), but enable investigations about how the complicated neural morphology, the ionic conductance compositions, and the synaptic input distributions influence the neuron's signal processing.

Nonetheless, the detailed compartmental model's core remains electro-centric, describing mainly the generation and propagation of electrical signals in the brain. Consequently, Bhalla pointed out that it is perhaps best to think of neuronal computation as a seamless blend of electrical and chemical signalling (Bhalla, 2014). Numerous neuronal functions are initiated, modulated or maintained by chemical signalling pathways: environmental signals are quite often transduced into neuronal signals through molecular reaction pathways; neurons mainly communicate through chemical synaptic transmissions; ionic or molecular diffusions and changes to cytoplasmic ionic concentrations can be typical feedback regulator for intracellular pathways; and neuronal functions are also subject to other chemical processes, including neuromodulations, homeostasis, metabolisms and housekeeping processes.

The electro-centric models lack the integration of chemo-centric systems' biochemical models, making them insufficient to explain how chemical signals influence neuronal signalling and communications (De Schutter, 2008). As a result, a detailed compartmental neuron model, no matter how complicated and realistic in morphology, cannot mimic a real neuron in its natural environment, where its input would be dynamically integrated from many chemical synaptic events from numerous pre-synaptic neurons. This realisation raises the question: If a single neuron's input and output relationships cannot be investigated concerning its natural environment, what are the fundamental hypotheses for these models and simulations to test about their information flow and processing, or the proposed emergence of intelligence?

Need for biomimetic "whole-cell" neuron models to study neural information processing
A neuron is a signal processor that transforms its input or multiple inputs to its electrical outputs, from the information processing viewpoint. Forty years ago, David Marr proposed that three analysis levels are needed for a comprehensive understanding of neural information processing: the computational, the algorithmic and the implementational levels (Marr, 1982). Out of these, the mechanistic implementations have continuously remained elusive (Herz et al., 2006). It is hoped that this becomes possible with the help of biologically-realistic neuron models.

The ideal biologically-realistic single neuron models should integrate both the electrical membrane properties and the chemical transduction pathways. The first chemical kinetic models for neural signalling were published several decades ago (Land et al., 1981). Many pioneering studies have since highlighted the importance of integrating the electrical and biochemical reaction events for improving understanding of neuronal signalling (Bhalla, 2011; Bhalla and Iyengar, 1999; Kotter and Schirok, 1999). A wide range of kinetic models of chemical signalling pathways for signal transduction (Klipp and Liebermeister, 2006), synaptic transmission and plasticity (Kim et al., 2013; Naoki et al., 2005; Smolen et al., 2012) have been constructed, with standardised open-source simulation packages enabling the reaction kinetics to be coupled with particle diffusion in realistic neuronal morphology (Stiles and Bartol, 2000; Vayttaden et al., 2004). These models primarily comprise subcellular structures, such as synapses, spines and dendrites, and can be analysed using dynamical systems approaches. But because the models are local, tuned for neural

sub-structures, they are inherently limited in quantifying the input-output relationship of a "whole-neuron"; thus, these models cannot explain neural information processing at the global (cellular) level.

Biochemistry models and biophysical models should be integrated across the entire cell membrane at multiple spatial scales; from synapses and spines at nanometer scales to action potential propagation along axons up to a meter scale. "Whole-cell" models are such biomimetic models, implementing microscopic molecular details to reproduce macroscopic "whole-cell" dynamical input-output behaviours (Goldberg et al., 2018). The ultimate aim of "whole-cell" dynamical models is to act as virtual *in silico* cells, accounting for the integrated function of numerous genes or known molecules (Tomita, 2001). Such methodology is contemporary in systems biology. Several whole-cell dynamical models have been reported to simulate gene networks or cellular metabolisms (Goldberg et al., 2018), and this approach is predicted to have real potential to make a powerful impact on molecular and systems biology, bioengineering and medicine.

Unfortunately, however, it is hard to interlink stochastically operating signalling pathways, ionic diffusion, and electrical dynamics, and there are only a few "whole-cell" models for analysing neural information processing. This sparsity stems from the incomplete data to constrain the biochemical dynamics in neural signalling and the neurons' complicated structural sophistication and connectivity. Therefore, it is a formidable challenge to accurately assess and quantify a neuron's real inputs in its natural environments. Advantageously, peripheral sensory neurons, especially the receptor neurons, directly face the environment, their input can be effectively characterised (van der Schaaf and van Hateren, 1996). As such, the first "whole-cell" neuron models were built for fly (*Drosophila*, *Calliphora* and *Coenosia*) photoreceptors (Song et al., 2012a). Photoreceptors populate the retina, the first neural layer of the eye, where they sample and transduce changes in environmental photon influx (light input) into electrical responses (neural output), initiating vision.

From the information processing perspective, abided by data processing inequality (Shannon, 1948), which states that any post-processing cannot increase information, photon sampling constitutes the absolute visual information bottleneck (Juusola and de Polavieja, 2003). Any information the photoreceptors lose cannot be recovered downstream. Consequently, it is vital to understand how a single photoreceptor samples and processes light information and the underlying mechanisms that determine its capacity to do so.

Furthermore, because of the unprecedented molecular, ultrastructural, electrophysiological knowledge about the phototransduction pathways, and because its quantal sampling dynamics were obtained from systematic *in* and *ex vivo* experimental and information-theoretical investigations (Goldberg et al., 2018; Hardie, 1991; Hardie and Minke, 1992; Hardie et al., 1993; Hardie and Postma, 2008; Hardie et al., 2001; Juusola and de Polavieja, 2003; Juusola and Hardie, 2001a, b; Juusola et al., 1994; Niven et al., 2003; Song et al., 2012b; Vähäsöyrinki et al., 2006; Wardill et al., 2012; Zheng et al., 2006; Zheng et al., 2009), fly photoreceptors became the premier "whole-cell" models for simulating neural information processing.

The "whole-cell" fly photoreceptor models are multiscale. For the first time to our knowledge, they connected the microscopic molecular reaction dynamics and the macroscopic "whole-cell" input-output transformations in a single simulation platform. The previous state-of-the-art biophysical fly photoreceptor models either focused on mapping the cell's steady-state nonlinear input-output relationships (French et al., 1993; Juusola et al., 1995b; van Hateren and Snippe, 2006) or simulating its molecular reaction pathways in transducing single photon energy (Pumir et al., 2008). In clear contrast, the "whole-cell" photoreceptor models (Song et al., 2012a) combined these two separate objectives. These new models accurately simulate the molecular reactions of a photoreceptor's sampling unit (microvillus) in transducing a single photon and the reaction dynamics of 30,000-90,000 microvilli when transducing millions of photons. And crucially, by following the experimentally quantified quantum bump (elementary response) dynamics and statistics (Gonzalez-Bellido et al., 2011; Juusola and de Polavieja, 2003; Juusola and Hardie, 2001a, b), these models could reliably reproduce continuous voltage responses with realistic variability to any light intensity time series, without the need to train any parameters (Juusola et al., 2017; Song and Juusola, 2014).

4

The "whole-cell" fly photoreceptor models enable information processing studies at the three levels of analysis. At the implementation level, they have been crucial in revealing novel light adaptation mechanisms, such as the subcellular refractory period (RP) and the signalling stochasticity (Song et al., 2012a). At the algorithmic level, they have paved the way for developing algorithms with only four sampling parameters to achieve automatic gain control and temporal adaptation (Song et al., 2017). At the computational level, they have elucidated phototransduction dynamics through a framework of refractory photon information sampling, leading to a trade-off between coding efficiency and energy consumption (Li et al., 2019; Song and Juusola, 2014). We next review the multiscale "whole-cell" fly photoreceptor models, specifically focussing on the *Drosophila* R1-R6 photoreceptor model and its emergent properties at these levels.

Drosophila R1-R6 "whole-cell" photoreceptor model

The first "whole-cell" model built for a neuron was a fly photoreceptor model (Song et al., 2009; Song et al., 2012b). The model simulates the cell's light response dynamics at multiple spatial scales. It linked the intracellular molecular dynamics with the "whole-cell" input-output relationships and was constructed to map light intensity time series input into a continuous voltage response at the cellular level. Light input mimics a photoreceptor's light-intensity-time-series input at its receptive field. Because light is composed of photons, the light intensity changes were quantified as photons/s (Juusola and de Polavieja, 2003; Juusola and Hardie, 2001a). For model validations, the simulations were compared to the corresponding real recordings. In *in vivo* recordings, the light intensity time series of specific statistics are played back to the photoreceptor using a feedback-controlled LED/light-guide-stimulator (Juusola and de Polavieja, 2003; Juusola and Hardie, 2001a; Zheng et al., 2006), while the resulting photoreceptor output, the voltage response to the light input, was recorded intracellularly using a sharp microelectrode in an intact living fly (Juusola et al., 2016; Juusola and Hardie, 2001a).

At the molecular level, the light input is quantal, with information carried by discrete photon arrivals. Photons are absorbed by rhodopsin-molecules (light-sensitive G-protein-coupled receptors) inside 30,000 microvilli (sampling units), each of which is a compartmentalised finger-like membrane protrusion. Together, the microvilli stack up the rhabdomere, the photosensitive part of the photoreceptor (Fig. 1A). Each microvillus contains a full G-protein-coupled receptor (GPCR) signalling pathway (Hardie and Juusola, 2015; Hardie and Postma, 2008), which constitutes a sequence of biochemical reactions called the phototransduction cascade (Fig. 1B). This cascade can transduce a single photon into a quantum bump (QB), a unitary analogue current influx (Hardie, 1991; Henderson et al., 2000; Juusola and Hardie, 2001a).

The first state-of-the-art phototransduction cascade model simulated the production of single QBs inside one microvillus (Pumir et al., 2008). Whereas the later R1–R6 photoreceptor models describe how 30,000 microvilli act in parallel, transducing millions of photons into thousands of QBs and integrating them into the macroscopic "whole-cell" light-induced-current (LIC) (Song et al., 2009; Song et al., 2012a). The macroscopic LIC then charge the photoreceptor's photo-insensitive membrane, generating a macroscopic voltage response (Li et al., 2019; Niven et al., 2003; Vähäsöyrinki et al., 2006) (Fig. 1C).

The "whole-cell" photoreceptor model structure

Akin to a real R1–R6 photoreceptor, the model comprises four biophysically realistic submodules (Fig. 1D) (Juusola et al., 2015; Song et al., 2012a):

- Random Photon Absorption Model (RandPAM) distributes the incoming photons to the 30,000 microvilli following Poisson statistics. Its output is the absorbed photon sequences of each microvillus (Song et al., 2012a; Song et al., 2016).
- Stochastic Bump Model: stochastic biochemical reactions inside a microvillus transduce the absorbed photon sequences to QB sequences (Pumir et al., 2008; Song et al., 2012a). This model comprises ~20 nonlinear ODEs and includes ~50 parameters, and describes the molecular dynamics of the GPCR signalling pathway inside a single microvillus (Fig. 1E). The model uses the Gillespie algorithm

(Gillespie, 1976), a discrete and stochastic method that explicitly simulates a system with few reactants.

- Summation Model: QBs from 30,000 microvilli integrate to the macroscopic light-induced current (LIC) response (Song et al., 2012a) (Fig. 1F).
- Hodgkin–Huxley Model of the photoreceptor plasma membrane. This module transduces LIC into voltage response by reproducing the voltage-gated K^+ conductance dynamics on the photon-insensitive membrane (Li et al., 2019; Niven et al., 2003).
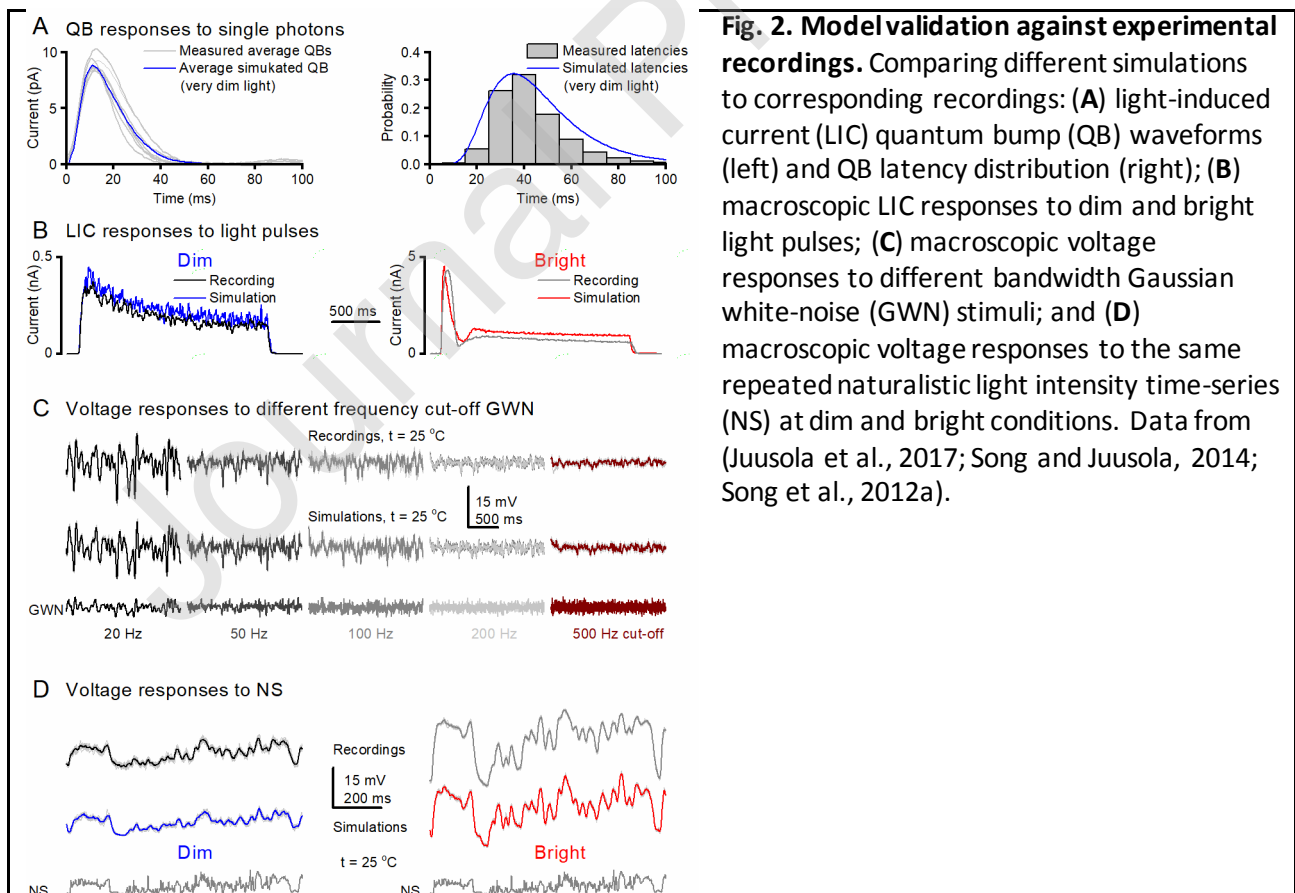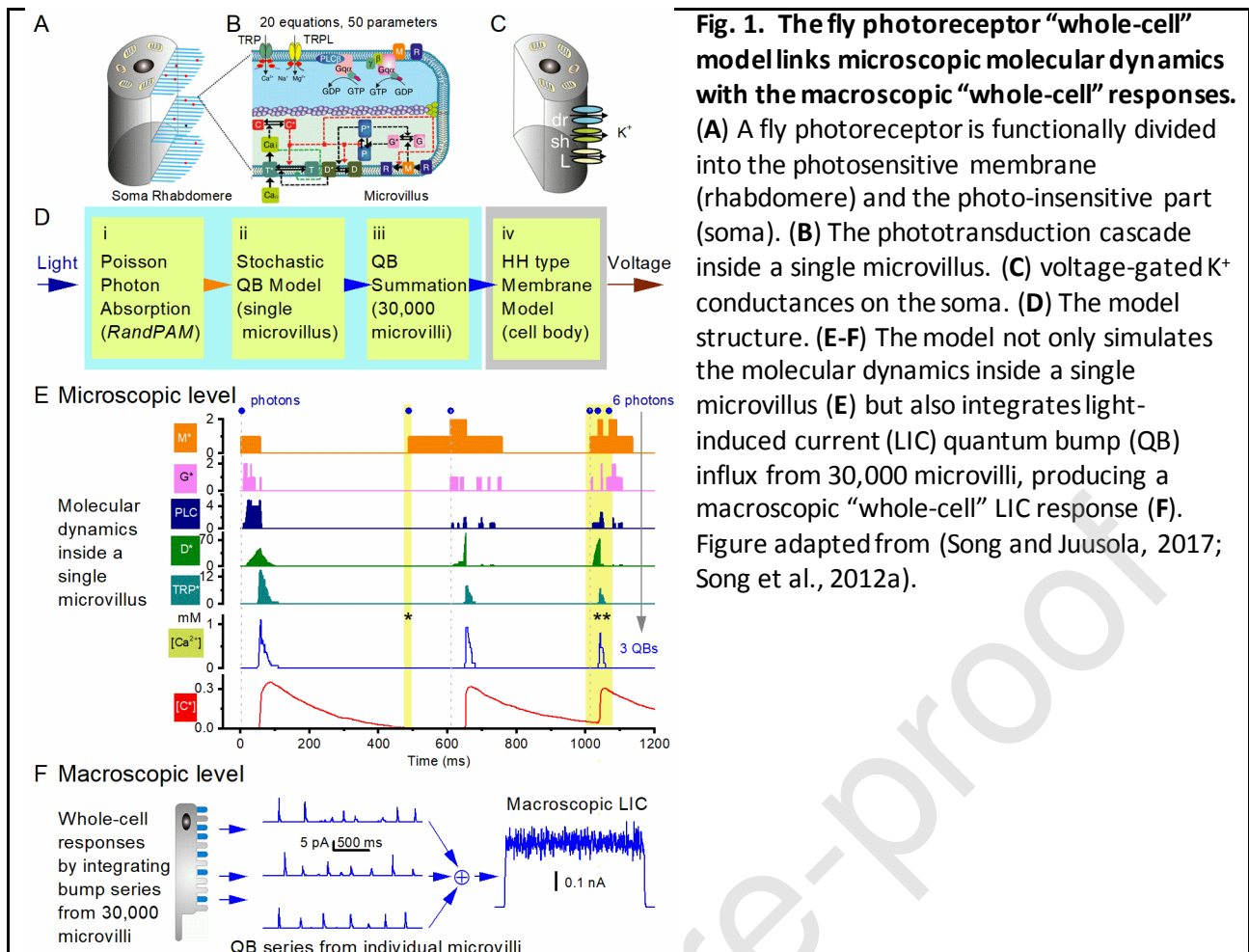
These modules were assembled and validated step-by-step to simulate QBs (Fig. 2A), the QB sequences inside a single microvillus (Fig. 1E), the photoreceptor's macroscopic responses to light steps (Fig. 2B), and light time series with various statistics (Figs. 2C and D). The model's continuous voltage responses were validated by the corresponding intracellular recordings (Juusola et al., 2017; Song and Juusola, 2014; Song et al., 2012a).

The "whole-cell" photoreceptor model samples information like a real photoreceptor
The "whole-cell" fly photoreceptor model surpasses other photoreceptor models in its generalisability and interpretability. The model is generalisable because it can predict responses to untested stimulus statistics. It retained its physiological relevance because the model parameters, wherever possible, were fixed to their physiologically measured or pre-estimated values (Juusola and Hardie, 2001a, b). The "whole-cell" fly photoreceptor model was first fitted to reproduce the cell's light impulse responses and step responses. Then, without refitting any parameters, the model was stimulated by other light time-series stimuli, including white noise with various bandwidth and naturalistic stimuli with 1/f power spectra. The model predicted realistic response waveforms to all tested stimuli, showing its great generalisability (Juusola et al., 2017; Juusola and Song, 2017; Song et al., 2009; Song and Juusola, 2017, 2014; Song et al., 2012a).

The "whole-cell" fly photoreceptor model is interpretable because it mechanistically describes how a photoreceptor's 30,000 microvilli (photon sampling units) sample light information in parallel, transducing millions of photons into thousands of QBs and integrating them into the macroscopic voltage responses (Song et al., 2009; Song et al., 2012a). Given that the model's QB statistics match those measured for the ambient light condition (Juusola et al., 2017; Juusola and Hardie, 2001a, b), the model produces similar voltage responses to the real recordings (Juusola et al., 2017; Song and Juusola, 2014; Song et al., 2012a). This equivalence signifies the whole-cell model's intrinsic accuracy in replicating a real photoreceptor's adaptive response dynamics from the photon sampling to QB integration.

Next, we will review how the whole-cell" photoreceptor model's generalisability and interpretability have contributed to scientific advancement in the insect vision field.

6

Fig. 1. The fly photoreceptor "whole-cell" model links microscopic molecular dynamics with the macroscopic "whole-cell" responses. (**A**) A fly photoreceptor is functionally divided into the photosensitive membrane (rhabdomere) and the photo-insensitive part (soma). (**B**) The phototransduction cascade inside a single microvillus. (**C**) voltage-gated K⁺ conductances on the soma. (**D**) The model structure. (**E-F**) The model not only simulates the molecular dynamics inside a single microvillus (**E**) but also integrates light-induced current (LIC) quantum bump (QB) influx from 30,000 microvilli, producing a macroscopic "whole-cell" LIC response (**F**). Figure adapted from (Song and Juusola, 2017; Song et al., 2012a).

Fig. 2. Model validation against experimental recordings. Comparing different simulations to corresponding recordings: (**A**) light-induced current (LIC) quantum bump (QB) waveforms (left) and QB latency distribution (right); (**B**) macroscopic LIC responses to dim and bright light pulses; (**C**) macroscopic voltage responses to different bandwidth Gaussian white-noise (GWN) stimuli; and (**D**) macroscopic voltage responses to the same repeated naturalistic light intensity time-series (NS) at dim and bright conditions. Data from (Juusola et al., 2017; Song and Juusola, 2014; Song et al., 2012a).

7

"Whole-cell" fly photoreceptor model elucidate generic encoding rules

Quantal sampling dynamics govern adaptation

With the real-world objects looking broadly the same from dawn till dusk, visual animals can execute successful behaviours. Much of this invariance comes from the physical objects' invariable relative reflectance, which vision encodes into perceptual contrast constancy. Remarkably, insect photoreceptors already show early contrast constancy by generating similar response waveforms to the same naturalistic stimulus from dim to ~1,000,000-times brighter conditions (Faivre and Juusola, 2008; Friederich et al., 2009; Gonzalez-Bellido et al., 2011; Juusola and de Polavieja, 2003; Zheng et al., 2006; Zheng et al., 2009) (Fig. 2D). The large dynamic range for encoding similar contrast responses within a photoreceptors' limited amplitude (~60 mV) and frequency range (~200-300 Hz) is achieved through light adaptation, the system's ability to change its sensitivity according to light intensity changes. In terms of absolute light detection, fly photoreceptors far surpass man-made sensors in achieving 8-10 orders of magnitude dynamic range (Howard et al., 1987; van Hateren, 1997).
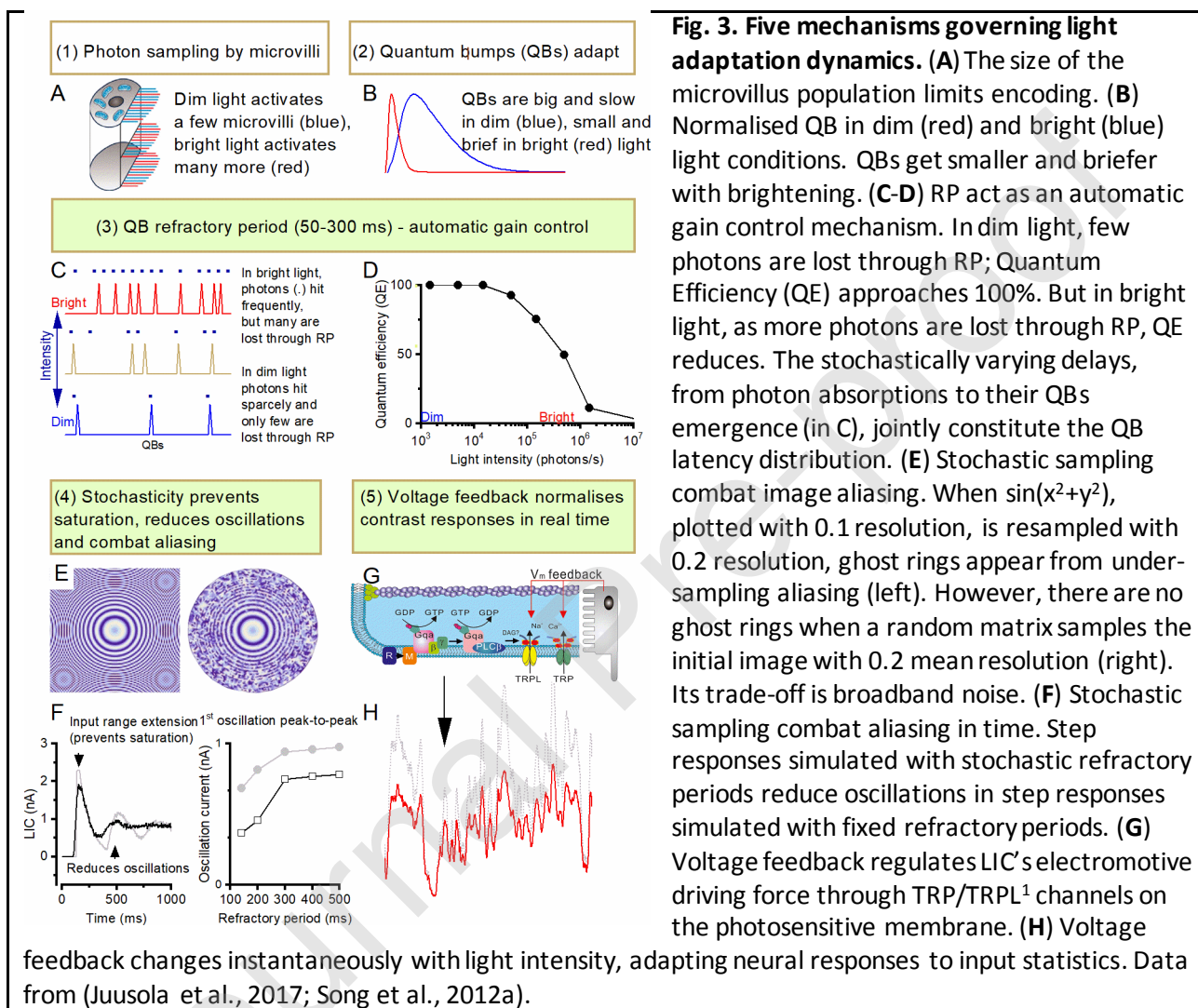
It has been widely studied how photoreceptors adapt over the day/night-cycle by various gain control mechanisms. But for effective visual course control, photoreceptors must also adapt continuously and near instantaneously to their local light intensity changes, which could be full of various temporal structures, as an animal locomotes within a natural scene (Clark et al., 2013; Juusola et al., 2017; Juusola and de Polavieja, 2003; Silva et al., 2001; Zheng et al., 2009).

How does a fly photoreceptor's adaption dynamics change within a millisecond-to-second time scale? The "whole-cell" *Drosophila* photoreceptor model provides a powerful simulation platform to investigate this question (Fig. 3). The model can produce realistic photoreceptor responses at vastly varying light conditions and has elucidated four factors that control fast adaptation. These are: (i) the number of microvilli in the rhabdomere, the photosensitive structure; (ii) QB size (waveform); (iii) QB latency distribution (latency is the delay between a photon arrival and its QB emerging), and (iv) RP distribution in a microvillus, (its recovery time after a QB) (Song and Juusola, 2014; Song et al., 2012a). These factors constitute a set of rules, which jointly govern a photoreceptor's light adaptation and information sampling dynamics:

- Population sampling; the microvillus population size sets the encoding limit (Fig. 3A). The number of microvilli (photon sampling units) is the critical parameter, limiting a photoreceptor's encoding capacity (Hochstrate and Hamdorf, 1990; Howard et al., 1987; Song and Juusola, 2014; Song et al., 2012a). Simulations, in which the microvilli amount and properties were systematically changed, demonstrated that the photoreceptors with the most and fastest microvilli generate the highest-fidelity responses (Juusola and Song, 2017; Song and Juusola, 2014; Song et al., 2012a), consistent with corresponding neuroethological, electrophysiological and ultrastructural data.
- Adaptive QB. QBs get smaller and briefer with brightening (Fig. 3B) and can shrink ~50 times from dark to bright (Juusola and Hardie, 2001a). This QB desensitisation is caused by the nonlinear biochemical reactions and the negative feedbacks within the phototransduction cascade.
- Microvillar RP. RP enlarges the dynamic range (Figs 3C-D) and contributes to temporal adaptation (Song et al., 2012a; Song et al., 2017). Simulations, in which a single microvillus responds to a photon sequence, established that each QB is followed by a 50-300 ms RP (Juusola et al., 2015; Song et al., 2012a). This RP is different from an action potential's RP, which affects the whole neuron at once. Whereas a microvillar RP is a local phenomenon. Only the microvilli, which generate QBs, become refractory. Because this happens across subcellular micro-domains (Song et al., 2017), the current recording techniques cannot measure it directly from the integrated response or QBs. Thus experimentally, it is difficult to assess how RP impacts encoding.

RP greatly benefits encoding in graded potential systems. The microvillar RP provides an automatic gain control mechanism, which enlarges the photoreceptor's dynamic range by two orders of magnitude (Song and Juusola, 2017; Song et al., 2012a). Some input information is inevitably lost through RP as some photons fail to evoke QBs, eventually saturating the QB count (Juusola et al., 2017; Song and Juusola, 2014; Song et al., 2012a). Nevertheless, for a *Drosophila* R1-R6, ~10^5-10^6 QBs/s in a bursty time series maximise

output information within its bandwidth, and increasing QB count any further makes little difference to its already lofty signal-to-noise ratio (>20,000) (Juusola et al., 2017). Refractoriness further accentuates responses to salient brightness changes (Juusola et al., 2017; Juusola et al., 2015; Song and Juusola, 2014; Song et al., 2012a). By enlarging response transients to light on- and offsets, it enhances the neural representation of phasic information, such as line elements and contrast edges (Friederich et al., 2016; Juusola and de Polavieja, 2003; Song and Juusola, 2014). Thus, using local refractory sampling units could be one general mechanism affecting adaptation and computations, as suggested by seemingly similar response dynamics of many sensory neurons and synapses (Juusola and French, 1997; Juusola et al., 1996; Juusola et al., 1995a; Rabinovich et al., 2008), and as already modelled for a mechanoreceptor's dynamic behaviour (Song et al., 2015).

Fig. 3. Five mechanisms governing light adaptation dynamics. (**A**) The size of the microvillus population limits encoding. (**B**) Normalised QB in dim (red) and bright (blue) light conditions. QBs get smaller and briefer with brightening. (**C**-**D**) RP act as an automatic gain control mechanism. In dim light, few photons are lost through RP; Quantum Efficiency (QE) approaches 100%. But in bright light, as more photons are lost through RP, QE reduces. The stochastically varying delays, from photon absorptions to their QBs emergence (in C), jointly constitute the QB latency distribution. (**E**) Stochastic sampling combat image aliasing. When $sin(x^2+y^2)$, plotted with 0.1 resolution, is resampled with 0.2 resolution, ghost rings appear from under-sampling aliasing (left). However, there are no ghost rings when a random matrix samples the initial image with 0.2 mean resolution (right). Its trade-off is broadband noise. (**F**) Stochastic sampling combat aliasing in time. Step responses simulated with stochastic refractory periods reduce oscillations in step responses simulated with fixed refractory periods. (**G**) Voltage feedback regulates LIC's electromotive driving force through TRP/TRPL[1] channels on the photosensitive membrane. (**H**) Voltage feedback changes instantaneously with light intensity, adapting neural responses to input statistics. Data from (Juusola et al., 2017; Song et al., 2012a).

Stochastic signalling: stochastic QB production anti-aliases temporal responses
Both photon absorptions and QB productions are inherently stochastic (Pumir et al., 2008; Song et al., 2016), and the term *stochastic sampling* was coined to describe the stochastic operation of the entire microvillus population (Song et al., 2012a). By employing the Gillespie algorithm (Gillespie, 1976) - to simulate the "whole-cell" photoreceptor model, its stochasticity could be mimicked realistically to investigate how QB variations impact information processing.

In contrast to the past view, where the QB variations were considered mostly noise that lowers a photoreceptor's information transfer (Laughlin and Lillywhite, 1982; Lillywhite, 1979; Lillywhite and Laughlin, 1979), both our modelling and experimental results indicate that stochasticity benefits encoding. The stochastically operating microvilli resist saturation in generating the macroscopic photoreceptor output

(Juusola et al., 2015; Song et al., 2012a). Stochastic QB latency distributions are similar over a wide range of light backgrounds (Juusola and Hardie, 2001a), weighting microvilli output to evoke similar-looking temporal responses to naturalistic stimulation in different illumination conditions (Faivre and Juusola, 2008; Juusola and de Polavieja, 2003).

Stochastic sampling may represent a generic solution to the temporal aliasing problems (Fig. 3E). Simulations show that stochastic refractory periods reduce oscillations in photoreceptor output compared to those seen in models with a fixed refractory period (Fig. 3F) (Song and Juusola, 2017; Song et al., 2012a). A more detailed account of how stochastic sampling benefits encoding and the related trade-off between anti-aliasing and broadband noise can be found in the recent publications (Juusola et al., 2017; Juusola and Song, 2017; Song and Juusola, 2017).

Global voltage feedback performs contrast normalisation
In the "whole-cell" photoreceptor model, voltages produced at the photo-insensitive membrane regulate the electromotive driving force of LIC through TRP/TRPL[1] channels on the photosensitive membrane (Fig. 3G) acting as global feedback (Song et al., 2012a). Although the concept of regulating an ion channel's driving force by voltage is not new (Hodgkin and Huxley, 1952), how this influences adaptation, especially to naturalistic stimulation, was less clear.

Simulations showed that the voltage regulation act as a global adaptive gain controller, compressing LIC signals less in dim conditions but far more to bright stimulation (Song et al., 2012a). Importantly, the feedback signal changes instantaneously as the light changes, adapting the neural responses to input statistics (Juusola and Song, 2017; Wark et al., 2007). This dynamic contributes to the rapid normalisation of a photoreceptor's contrast responses in a natural environment (Figs 2D and 3H) (Heeger, 1992; Juusola and de Polavieja, 2003; Li et al., 2019).

Together, the above mechanisms constitute *stochastic adaptive sampling* (Song et al., 2012a). Within this scheme, subcellular RP and stochastic signalling were found extremely beneficial for encoding efficient and invariable neural representations of the visual world. In contrast, these two mechanisms were previously thought to be detrimental to analogue signalling, as they either lose information or add noise. However, "whole-cell" model simulations have shown their real importance in elucidating how stochastic sampling maximises visual information packaging in photoreceptor output while minimising aliasing. For more in-depth reviews, please see (Juusola and Song, 2017; Song and Juusola, 2017).

Neuroethological adaptations
Different fly species have evolved with distinct behaviours and lifestyles. The fast-flying *Coenosia* is a predator, and the slow-flying *Drosophila* can be its prey (Gonzalez-Bellido et al., 2011). Starting from the photoreceptors, predatory *Coenosia* has faster vision than its fruit-loving cousin, *Drosophila*. What neuroethological adaptations give *Coenosia* faster photoreceptor dynamics and vision?

"Whole-cell" photoreceptor models can be tweaked to predict the responses of different fly species. The same model structure works equally well for simulating *Drosophila*, *Coenosia* and *Calliphora* photoreceptor responses, with the changes in the four QB sampling factors accounting for most of their differences (Fig. 4). The fast-flying flies can have more microvilli, briefer QBs, smaller RPs and narrowed latency distributions (Song and Juusola, 2014; Song et al., 2012a). These findings suggest that evolution may use conserved computational adaptation mechanisms to match early visual information processing with lifestyles.

---

[1] TRP: Transient receptor potential; TRPL: Transient receptor potential like;

TRP channels were initially discovered in the so-called "transient receptor potential" mutant (trp-mutant) strain of the fruit fly *Drosophila*, hence their name. Later, TRP channels were found in vertebrates where they are ubiquitously expressed in many cell types and tissues (Hardie, 2007).
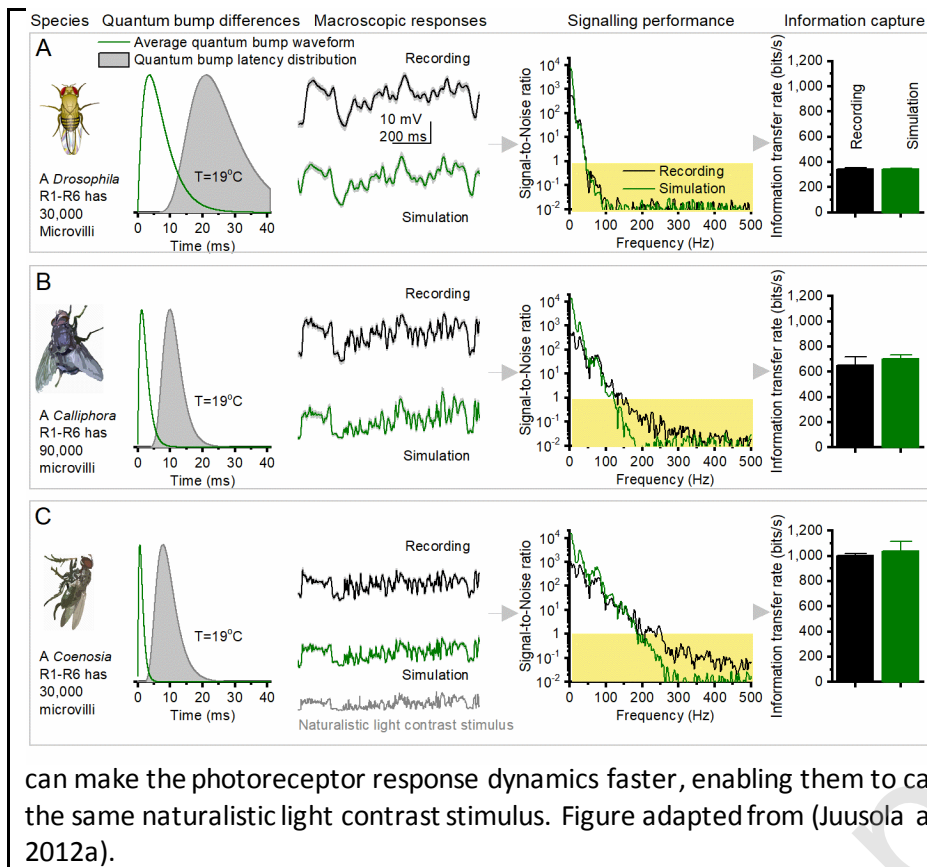
Fig.4. Neuroethological adaptation differences in fly photoreceptor voltage responses. Different fly species have evolved with distinct visual behaviours and lifestyles. The same model structure can accurately predict R1-R6 photoreceptor voltage responses and their information transfer rates of slow-flying (**A**) *Drosophila melanogaster* and fast-flying *Calliphora vicina* (**B**) and *Coenosia attenuata* (**C**). Larger microvillus population, smaller bumps, narrower latency distribution and shorter refractory periods can make the photoreceptor response dynamics faster, enabling them to capture more information from the same naturalistic light contrast stimulus. Figure adapted from (Juusola and Song, 2017; Song et al., 2012a).

Algorithmic photoreceptor signalling implementation

John von Neumann famously proclaimed: *With four parameters I can fit an elephant, and with five I can make him wiggle his trunk* (Mayer et al., 2010), meaning that a complex model with enough parameters can fit any data and perhaps one should not be too impressed by that.

One can argue that the "whole-cell" photoreceptor models are too complicated with too many details, containing too much or unnecessary parts. But through their systematic construction and testing against comparable experimental recordings, the models have played a significant role in revealing a new understanding of how the fly photoreceptors sample light information (Juusola et al., 2017; Song and Juusola, 2014; Song et al., 2012a). This new understanding then helped to reduce the "whole-cell" model into a much simple phenomenological model, incorporating as little parameters as possible while being inspired by the earlier ideas about quantal sampling (Henderson et al., 2000; Juusola et al., 2016; Juusola and Hardie, 2001a, b; Juusola et al., 1994; Juusola et al., 1995a; Wong and Knight, 1980; Wong et al., 1982, 1980). The new idea was to probabilistically sample QBs from the latency distribution and the newly discovered refractory distribution (Song et al., 2017). The resulting reduced 4-parameter model can predict the photoreceptor response dynamics equally well with the "whole-cell" model (Li et al., 2019; Song et al., 2017).

The reduced model is parameterised into four sampling factors: the microvillus (sampling unit) count, QB waveforms, QB latencies, and QB RPs, while its four-parameter algorithm design is based on stochastic renewal processes. It is assumed that the QB generations inside a microvillus follow a renewal process, and superpositions of 30,000 independent renewal processes are used to model photoreceptor signalling. The model implements five rules: (1) A microvilli population absorbs photons based on Poisson processes. (2) Each successfully absorbed photon leads to a delayed QB. (3) A refractory period follows each QB. (4) All QBs sum up macroscopic LIC. (5) QB latencies and refractory periods are stochastic variables that follow long-tailed distributions, e.g. log-normal distributions.

This simple model is important because:

- From the systems biology perspective, the simple model acts as a mesoscopic bridge to link the molecular dynamics at the microscopic level to the "whole-cell" response at the macroscopic level, which otherwise would be hard to do; owing to the complicated interconnections within the molecular reaction network.
- Extensive computer simulations may help to obtain qualitative insight, but it is the mathematics that truly delineates the system. Mathematical analysis for quantitative results is easier to perform on the simple model. A new formula was defined to calculate the probability density function (PDF) for the QB interval distribution: *not* the convolution of the PDF of the photon-interval and the RP's PDF, but the weighted sum of the two (Song et al., 2017). In the past research, it was unconsidered that photons could arrive after the RP, in which case the RP does not influence encoding (Franklin and Bair, 1995).
- The simple model is an algorithmic implementation of the photoreceptor signalling, accomplishing the 2nd level in the three analysis levels. Such algorithms can be beneficial in brain-inspired computations.

Refractory information sampling benefits vision

Light intensities in a natural scene are distributed in a highly structured way, showing strong spatiotemporal correlations (Juusola and de Polavieja, 2003; Rieke and Rudd, 2009; van Hateren, 1997). The efficient coding hypothesis proposes that the sensory neurons, networks and organs have evolved to utilise such environmental regularities in their neural representations (Barlow, 1961). Experiments have shown that sensory neurons transmit more information when the input stimuli are chosen from natural ensembles (Juusola and de Polavieja, 2003; Rieke et al., 1995). This realisation means that these neurons are not simple pre-processing filters. Otherwise, they would sample and transmit maximum information from a Gaussian white noise stimulus (GWN), which has a "flat" power spectrum and should contain most information within its bandwidth and variance (Juusola and de Polavieja, 2003; Shannon, 1948).

Why and how does an early sensory neuron encode various stimuli with different efficiency? What stimuli excite the neuron the most, producing the highest signal-to-noise ratio? These questions were investigated by "whole-cell" photoreceptor model simulations to GWN stimuli with different frequency cut-offs and manipulated naturalistic light time series, which follow different temporal statistics (Figs 5 and 6). (Juusola et al., 2017; Song and Juusola, 2014).

Four types of stimuli were used to simulate the "whole-cell" model:
(1) a naturalistic stimulus, NS, selected from van Hateren natural stimulus collection (Juusola and de Polavieja, 2003; van Hateren, 1997). The NS has complicated higher-order correlations, with neighbour values more likely to be similar, but its amplitude power spectrum roughly follows 1/f statistics.
(2) A shuffled-NS, having all NS intensity values rearranged in a random order to whiten the NS (Song and Juusola, 2014).
(3) An artificial GWN-1/f stimulus; a random phase-shifted NS (Song and Juusola, 2014).
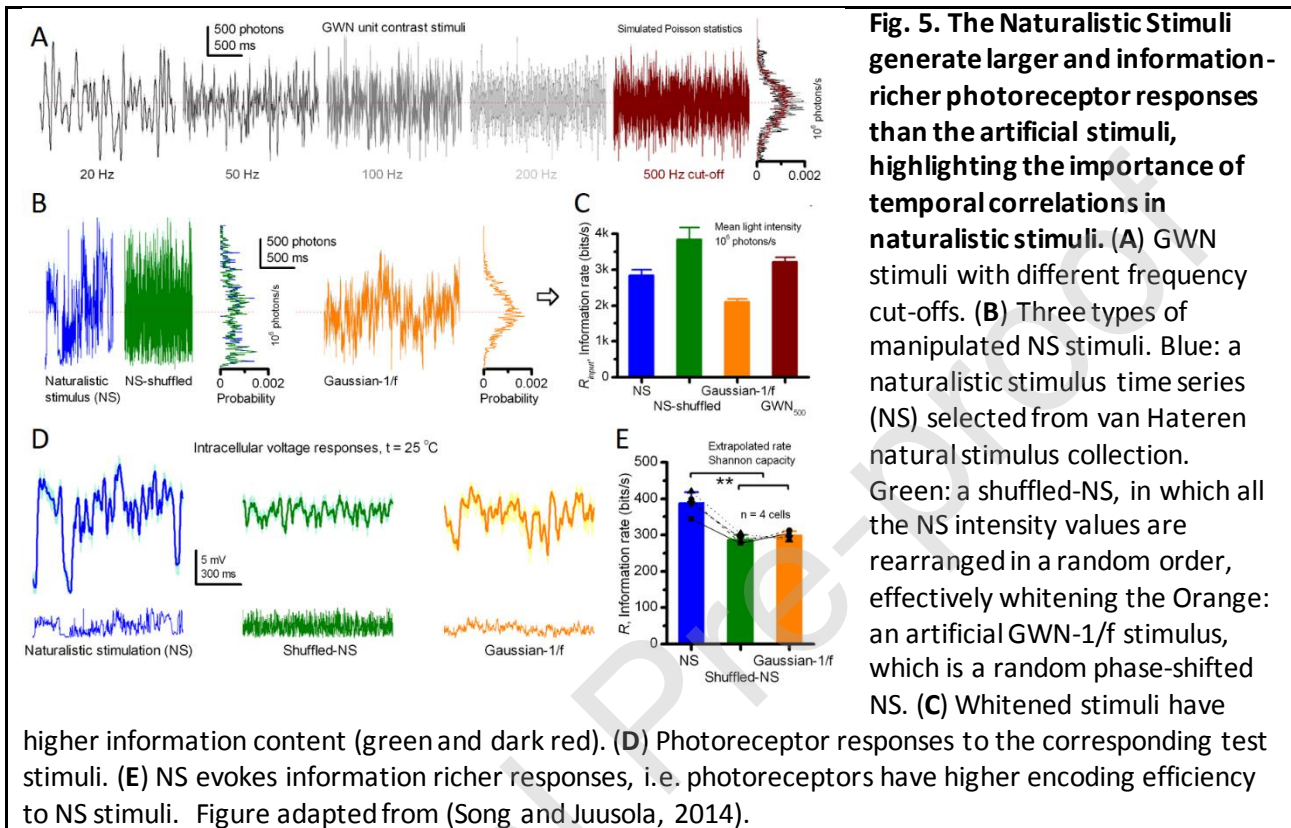(4) NS, modulated by a *Drosophila*'s saccadic walk within a natural scene (Juusola et al., 2017).

In each case, the model simulations closely resembled *in vivo* intracellular voltage responses to the very same stimuli. Thus, these conclusions were drawn:
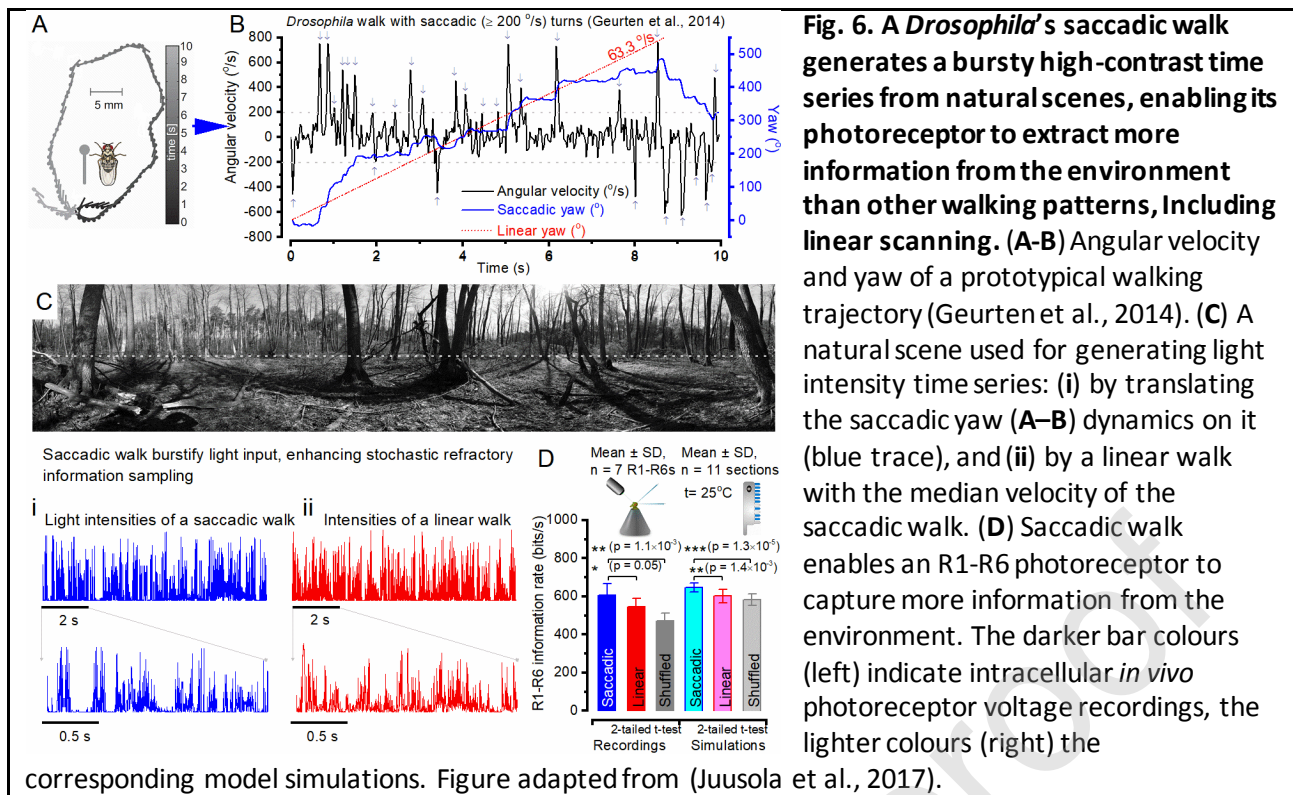
- Naturalistic stimulation generates larger and information-richer photoreceptor responses than stimuli without its temporal correlations (Juusola and de Polavieja, 2003; Song and Juusola, 2014). A *Drosophila* R1-R6 photoreceptor captures 2-to-4-times more information than previous maximum estimates (Juusola et al., 2017). In particular, this happens when a photoreceptor responds to high-contrast bursts (periods of rapid bright light changes followed by darker quiescent periods) that resemble light input from natural scenes generated by saccadic viewing (Fig. 6). These results explain why GWN, which lacks all these correlations, is a highly inefficient stimulus to study neural performance.
- The mechanistic reason why information sampling is more efficient for NS stimulation is that a photoreceptor's information capture depends critically upon the stochastic refractoriness of its 30,000 sampling units (microvilli). NS contains more dark contrasts (Ratliff et al., 2010), recovering more

12

refractory microvilli (Juusola et al., 2017; Juusola and Song, 2017; Song and Juusola, 2014). The more available microvilli enable the cell to sample more photons, generating more QBs, from phasic light changes, and encoding more information (Juusola et al., 2017; Song and Juusola, 2014).

● Stochastic refractory periods also lower the cell's metabolic costs. For a bright NS stimulus, 40% of energy is saved by losing 12% of information (Song and Juusola, 2014).

In summary, at the computational level of analysis, the phototransduction process can be understood through a framework of refractory photon information sampling. The results provided mechanistic reasons why and how the earliest neural code and metabolic cost depend upon the stimulation's statistical context.

Fig. 5. The Naturalistic Stimuli generate larger and information-richer photoreceptor responses than the artificial stimuli, highlighting the importance of temporal correlations in naturalistic stimuli. (**A**) GWN stimuli with different frequency cut-offs. (**B**) Three types of manipulated NS stimuli. Blue: a naturalistic stimulus time series (NS) selected from van Hateren natural stimulus collection. Green: a shuffled-NS, in which all the NS intensity values are rearranged in a random order, effectively whitening the Orange: an artificial GWN-1/f stimulus, which is a random phase-shifted NS. (**C**) Whitened stimuli have higher information content (green and dark red). (**D**) Photoreceptor responses to the corresponding test stimuli. (**E**) NS evokes information richer responses, i.e. photoreceptors have higher encoding efficiency to NS stimuli. Figure adapted from (Song and Juusola, 2014).

13

Fig. 6. A *Drosophila*'s saccadic walk generates a bursty high-contrast time series from natural scenes, enabling its photoreceptor to extract more information from the environment than other walking patterns, Including linear scanning. (**A-B**) Angular velocity and yaw of a prototypical walking trajectory (Geurten et al., 2014). (**C**) A natural scene used for generating light intensity time series: (**i**) by translating the saccadic yaw (**A–B**) dynamics on it (blue trace), and (**ii**) by a linear walk with the median velocity of the saccadic walk. (**D**) Saccadic walk enables an R1-R6 photoreceptor to capture more information from the environment. The darker bar colours (left) indicate intracellular *in vivo* photoreceptor voltage recordings, the lighter colours (right) the corresponding model simulations. Figure adapted from (Juusola et al., 2017).

Scalable "whole-cell" models: augmented new modules contribute to new discoveries

Many signalling pathways for diverse functions exist in cell physiology. There may be many dynamical processes that span over multiple spatial and temporal scales, even for a specific signalling process. The depth of knowledge may not be complete at any time to model all the processes in a cell. Therefore, a "whole-cell" model should be scalable. They should integrate new modules as the knowledge accumulates over time (Goldberg et al., 2018).

We have scaled up the "whole-cell" *Drosophila* photoreceptor model with two separate processes, including a module for microsaccadic photomechanical photoreceptor contraction dynamics (Juusola et al., 2017) and a module to infer the cell's synaptic feedback currents (Li et al., 2019). These new augmented modules have helped to obtain new understandings about insect vision and synaptic homeostasis. Such development shows that when a "whole-cell" model is constructed from biophysically realistic modules, as new evidence accumulates, the emerging discrepancies between the model predictions and experimental observations may indicate knowledge expansion opportunities.

Photomechanical Photoreceptor microsaccades combat motion-blur and induce hyperacuity

Whilst light adaptation enlarges the eye's dynamical range, it also desensitises the eye over time, causing perceptual fading to the unchanging visual stimulus. For example, this happens when nothing moves within a scene, and the gaze is held completely still (Ditchburn and Ginsborg, 1952). To refresh the retinal image and prevent it from fading, animals make rapid involuntary eye movements called microsaccades (Ahissar and Arieli, 2012). It was not known why microsaccades do not blur vision (Packer and Williams, 1992).

This question could be addressed by systematically striving to replicate experimental *in vivo* recordings with the "whole-cell" *Drosophila* photoreceptor model simulations (Juusola et al., 2017). Using *ex vivo* atomic force microscopy, Hardie and Franze (2012b) had found earlier that *Drosophila* photoreceptors contract photomechanically. They proposed how these nanoscale twitches contribute to light-sensitive channel gating but thought these movements were too small to affect vision. However, *in vivo,* high-speed optical microscopy with electrophysiology revealed that targeted light stimulation causes a larger ultrafast axiolateral photoreceptor movement, a microsaccade (Fig. 7), which dynamically shifts and narrows its

receptive field (Juusola et al., 2017). These photomechanics, which simultaneously shape both the light input and photoreceptor output, could be modelled by a separate module, placed as a pre-processing step in the "whole-cell" model (Juusola et al., 2017).

The simulations were tuned to replicate *in vivo* electrophysiological recordings, in which two bright spatially separated dots crossed a photoreceptor's receptive field, generating a highly-phasic two-peaked voltage response (Fig. 7Biv). With the recordings and model predictions being consistent with the related *in vivo* behavioural tests and controls, it became clear that photoreceptor microsaccades significantly improve *Drosophila*'s ability to see in fine-resolution fast-moving objects (Juusola et al., 2017). Thus, microsaccades effectively reduce motion blur, sharpening the retinal image to separate adjacent visual objects in time. This active sampling mechanism allows *Drosophila* to see >4-folds finer details than their hypothesised optical pixelation limit (interommatidial distance), disproving the 100-year-old theory about compound eye acuity (Juusola et al., 2017).
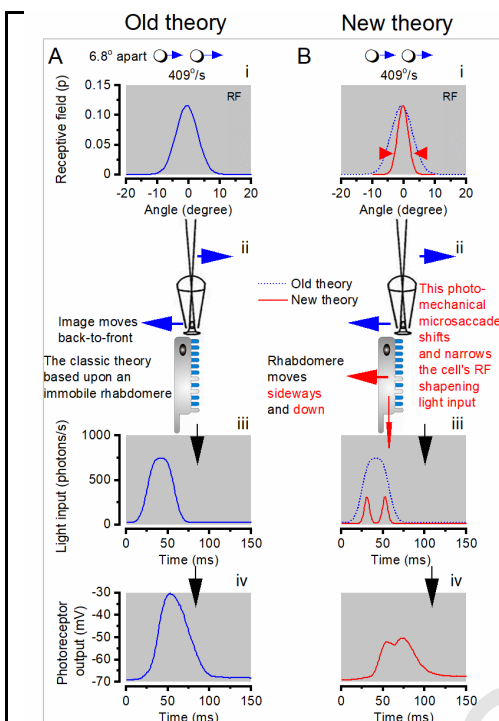
Fig. 7. Microsaccadic eye movements increase visual acuity in insect vision. A microsaccadic movement model was developed to tune the light input for the photoreceptor model. This model allows the photoreceptor's receptive field to move and narrow with the moving dots. (**A**) According to the old theory, because the photoreceptor has a broad Gaussian receptive field (RF, blue, **i**), which stays still (**ii**), two bright dots crossing across it fast cannot be resolved (**iii** and **iv**). (**B**) According to the new theory, when the dots touch the edge of the RF (**i**), the photoreceptor's light absorption causes it to contract (**ii**). This microsaccade moves and narrows the RF (**i**, red), sharpening light input (**iii**, red) so that the two moving dots can be encoded in time as two separate peaks in the voltage response (**iv**). Figure adapted from (Juusola et al., 2017).

Synaptic feedback: photoreceptor-interneuron-photoreceptor circuit homeostasis
Homeostatic processes regulate neurons' electrical activity and make circuitry communication fault-tolerant against perturbations (Marder and Goaillard, 2006). Nevertheless, such robustness could have associated costs (Abbott and Lemasson, 1993). How do the intrinsic perturbations of missing Ca^{2+} activated K^+ channels influence the synaptic transmission, and what are the costs? These questions can be investigated by studying the synaptic transmission between photoreceptors and interneurons (Large Monopolar Cells or LMCs). In this R-LMC-R system, stereotypical columns of feedforward and feedback synapses are formed to process and route visual information to the *Drosophila* brain (Dau et al., 2016; Meinertzhagen and O'Neil, 1991; Rivera-Alba et al., 2011; Zheng et al., 2006; Zheng et al., 2009).

The R-LMC-R circuitry is perturbed by gene deletions in SK, "small", and BK, "big", conductance Ca^{2+}-activated K^+-channels. One can work out how these channels contribute to neural processing by systematically comparing intracellularly recorded and "whole-cell"-model-simulated wild-type and mutant photoreceptor voltage responses to naturalistic light intensity time series (Li et al., 2019; Zheng et al., 2006). Furthermore, because the original photoreceptor model lacked the synaptic feedback conductances, the differences between the simulated and recorded responses could be used to infer how these shape photoreceptor voltage responses (Fig. 8). By directly comparing the model predicted photoreceptor responses (without the synapse) to the real photoreceptor recordings for the same light stimulation, we could work out how the synaptic feedback modulation (from LMCs) accentuates the photoreceptor output,

15

and how this modulation happens homeostatically as the mutant flies' photoreceptor-LMC-photoreceptor systems adapt their synaptic loads. This approach gave computational means to quantify the homeostatic changes involved and their cost in retaining synaptic information transfer (Li et al., 2019).

The R-LMC-R circuitry shows real robustness: the loss of SK and BK channels did not diminish *Drosophila* photoreceptors' information sampling and transmission capacity *in vivo*. However, the homeostatic compensation did come with unavoidable costs. It reduced other K^+-currents and overloaded synaptic feedback from the lamina network, reshaping fast adaptation trends in photoreceptor output. In effect, communication between the mutant photoreceptors and LMCs became inefficient, consuming more energy while distorting visual information flow to the brain. Thus, the results indicated that whilst homeostatic compensation makes neural communication robust, this comes with the price tag of being energetically more expensive and less adaptive to sudden large light changes (Abou Tayoun et al., 2011; Li et al., 2019).
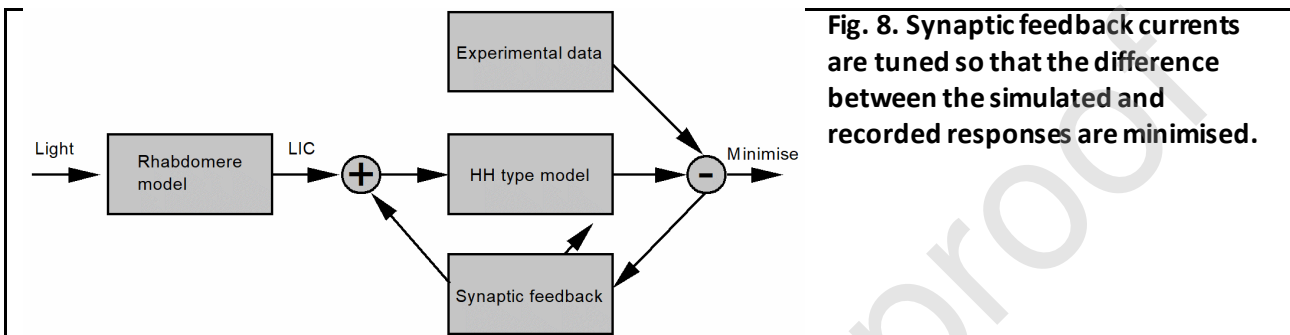
Fig. 8. Synaptic feedback currents are tuned so that the difference between the simulated and recorded responses are minimised.

Conclusion

"Whole-cell" models are bottom-up models, which - in their extreme form - aim to account for the integrated function of every gene or molecule inside a cell. They integrate heterogeneous dataset about the studied organism into a unified simulation framework for systematic investigations. Such models for bacteria have already shown their capacity to predict complex cellular dynamics, identify knowledge limitations, and suggest future experiments for obtaining new knowledge (Carrera and Covert, 2015). However, in computational neuroscience, there has been a void for "whole-cell" neuron models that can (1) integrate both biochemistry models for signalling pathways and biophysical models for the electrical behaviours of the membrane; (2) perform the integration at the "whole-cell" cellular level across many spatial scales, synapses- soma-axons; and (3) can reliably map the neuron's naturalistic inputs to its voltage responses at the cellular level, for the study of neural information processing.

This gap was narrowed by constructing "whole-cell" fly photoreceptor models (Juusola and Song, 2017; Juusola et al., 2015; Song and Juusola, 2017; Song et al., 2012a). We reviewed these models and showed how they had been used to study insect vision and visual information processing. The current models were refined over many years and represent the latest knowledge of quantal light information sampling in microvillar compartmentalised phototransduction systems. These models can integrate the molecular dynamics of biochemical reactions at the microscopic scales and reproduce many experimentally observed dynamics or theoretically deduced mechanisms at the single-cell level. By simulating the dynamics of the contributing components, the models have revealed their considerable explanatory power in clarifying our understanding of various phenomena, such as (1) how to achieve contrast constancy – with objects looking the same in dim and bright conditions - through quantal *stochastic adaptive sampling* mechanisms (Juusola and Song, 2017; Juusola et al., 2015; Song et al., 2012a); (2) how this relates to photoreceptors' vast dynamic range (Song and Juusola, 2017; Song et al., 2012a; Song et al., 2017); and (3) how the photoreceptor microsaccades combat motion-blur, rather than cause it, enabling the flies to see visual details beyond their compound eye's optical limit (Juusola et al., 2017).

Without automatic parameter tuning, the model can respond like a real neuron to light time series that follow a wide range of statistics, as validated experimentally (Juusola et al., 2017; Song and Juusola, 2014).

The close match between simulations with experiments allows one to explore how the neuron processes stimuli with complex temporal correlations. Fly photoreceptors are incredibly well adapted to deal with fluctuating patterns of light that enter the eye, effectively utilising the structures of naturalistic light changes to maximise visual information sampling (Juusola et al., 2017; Song and Juusola, 2014). Through photomechanical microsaccades, they auto-regulate the light stimuli falling within their receptive fields, and by that, practically initiate active sensing (Juusola et al., 2017). These findings challenge the traditional ideas of photoreceptors being simple light detectors and the concept that the "real" vision only happens downstream in the retinal networks and within the brain.

"Whole-cell" models enable dissection of neural information processing at three levels of analysis. At the implementation level, they can be used to assess light-adaptation results from dynamic changes in quantal sampling (Song and Juusola, 2014; Song et al., 2012a). At the algorithmic level, the workings of a complex "whole-cell" model could be reduced to a simple algorithm with only four parameters to achieve automatic gain control and temporal adaptation (Song et al., 2017). At the computational level, the phototransduction process could be understood mechanistically through a framework of stochastic adaptive photon sampling, which clarified why coding of naturalistic stimuli with complex temporal correlations is more efficient than encoding GWN stimuli that lack these correlations (Juusola et al., 2017; Song and Juusola, 2014).

The success of these models is a direct testament to a close marriage between experiments and theory. Painstakingly perfected experimental methods provided intracellular neural responses and photomechanical contraction dynamics of wild-type and mutant flies with unprecedented quality (Hardie, 1991; Juusola et al., 2017; Juusola et al., 2016; Juusola and Hardie, 2001a; Song and Juusola, 2014), which could directly guide the model parameters (Juusola et al., 2017; Li et al., 2019; Song et al., 2009; Song and Juusola, 2014; Song et al., 2012a) and be used in the result comparisons. Simultaneously, information theoretical and systems analytical methods with minimal assumptions (Juusola and de Polavieja, 2003; Juusola and Hardie, 2001a; Shannon, 1948; Song et al., 2017; van Hateren and Snippe, 2006) enabled recordings and simulations (of the same size and resolution) to be tested and analysed in unbiased ways. From our experience of building and exploring with these "whole-cell" models, we found this integrative (multidisciplinary constructionist) approach extremely useful and would like to call for more efforts in this direction. Whole-cell models of more complex neurons need to integrate efforts from targeted experiments, computer simulations, theoretical hypothesis and mathematical descriptions, and thus inevitably will require interdisciplinary research cooperation.

Appendices

Appendix A：Some conceptual clarifications

"Whole-cell" models. Throughout this paper, "whole-cell" is printed in quotations, as the described photoreceptor models do not fall within the strict classification of including all signalling pathways. The fly photoreceptor models focus on the phototransduction signalling dynamics and ignoring other functions, such as gene encoding, protein synthesis and degradation, transcriptional regulation and metabolism. The models are not as complicated as the ones reported in systems biology; for example, the *M. genitalium* model implements 28 pathways (Goldberg et al., 2018). So "whole-cell" is used in a broader sense, indicating that a dynamical process is modelled both in the microscopic gene/molecular and macroscopic whole-cell scales.

Multi-modular, multi-compartmental and multiscale models. Several concepts can describe complex models: multi-modular models, multi-compartmental models, and multiscale models. We have encountered them all in our modelling process. Although the three concepts have different definitions, they can also intertwine with each other.

A multi-modular model is one where the organism or the model can be divided into different components. Each of these can be a sub-model for a different function. For example, a "whole-cell" photoreceptor model contains four modules, with each describing a different dynamical process; including the light absorption process, the stochastic molecular reaction pathway, and the deterministic membrane charging

process. A multi-compartmental model can encompass different body sections. In computational neuroscience, multi-compartmental models are used to account for the complex morphology of a neuron (Herz et al., 2006), and a complicated model can include tens of thousands of neural compartments. The "whole-cell" photoreceptor models have two major compartments: the photosensitive rhabdomere and the photo-insensitive cell body (Fig. 1). The photosensitive rhabdomere can be further divided into 30,000 microvilli. However, this part of the model only contains three modules, where the photo-insensitive compartment has only one module.

Multiscale models integrate models at different scales to describe a system with features that can happen at multiple space and time scales. The different models usually focus on different resolution scales, such as atoms, proteins, chemical reaction-diffusion or network dynamics. In computational neuroscience, there are systems models for neural circuitry, where signals from many neurons are pooled together as excitation or inhibition signals (van Vreeswijk and Sompolinsky, 1998). There are also single neuron models at various abstraction levels (Herz et al., 2006), including point-neuron models (Hodgkin and Huxley, 1952); morphologically-detailed multi-compartmental neuron models (Rall, 1959); subcellular models, described by differential equations (Izhikevich, 2004); and molecular dynamics models simulated with Monte Carlo methods (Vasudeva and Bhalla, 2004).

By definition, a "whole-cell" model is multiscale, integrating dynamics at many spatial and temporal resolutions. The "whole-cell" photoreceptor models are multiscale models that integrate intracellular protein level signalling with whole-cell level membrane electrophysiology. However, multiscale models do not need to be integrated into one complex model. Instead, they can be parallel models constructed down to different levels of abstraction. The three-levels-of-analysis framework is multiscale by nature, and we showed how the photoreceptor models could be analysed at the computational, algorithmic and implementation level.

Appendices B-E: Brief mathematical presentations of the "whole-cell" model

Akin to a real R1–R6 photoreceptor's signal transduction process, the "whole-cell" fly photoreceptor model comprises four biophysically realistic submodules (Fig. 1D) (Juusola et al., 2015; Song et al., 2012a). We now briefly present the mathematical summary of the model equations for the relevant modules so that this review is self-contained. The other details, such as the parameter justifications and the relevant experimental measurements, can be found in corresponding references. The Matlab scripts for this model are downloadable from the repository:
https://github.com/JuusolaLab/Microsaccadic_Sampling_Paper/tree/master/BiophysicalPhotoreceptorModel.

Appendix B: Random Photon Absorption Model (RandPAM)

Appendix B describes the Random Photon Absorption Model (RandPAM), which distributes the incoming photons to the 30,000 microvilli following Poisson statistics. Its output is the absorbed photon sequences of each microvillus (Song et al., 2012a; Song et al., 2016).

Assuming that all microvilli absorb photons independently and have the same photon absorption probability, the photon absorption process can be modelled as a multinomial process. At each time incident, the distribution of N_{ph} photons over N_u microvilli is multinomial with a size parameter equal to N_{ph}, and the probability vector of length N_u with each element equal to $\frac{1}{N_u}$.

Appendix C: Stochastic Bump Model

Appendix C shows the stochastic bump model (Song et al., 2012a). This model simulates the molecular reaction network for the fly phototransduction cascade, which transduces a sequence of absorbed photons to a sequence of unitary current events, called the quantum bumps, inside a single microvillus. Similar work can also be found in (Pumir et al., 2008), but it only simulates single-photon responses without the capability of simulating the transduction of photon arrival sequences. Simulation of bump sequences is needed for studying the light adaptation process.

The molecular reaction network is rather complicated, including a G-protein coupled receptor signalling pathway, various Ca^{2+} signalling pathways and the relevant feedback dynamics. A photon activates rhodopsin, which then kicks the G protein active, catalysing GDP exchange for GTP. The active Ga-GTP then couples to PLC and hydrolyses PIP_2 to generate DAG, $InsP_3$, and a proton. These reactions result in the activation of two classes of Ca^{2+} permeable cation channels, TRP and TRPL. Ca^{2+} influx via TRP then feeds back to multiple targets in the phototransduction cascade, including the channels, rhodopsin and PLC. The various feedbacks influence the light response kinetics, amplification and adaptation (refer to fig1 in Hardie and Juusola, 2015 for a pictorial representation of the pathway).

The model comprises ~20 coupled nonlinear ODEs with ~50 parameters (Fig. 1E). Because some of the reactant proteins are low in numbers, the model was simulated by a stochastic method, called the Gillespie algorithm, which generates the statistically correct solution of the underlying chemical master equation (Gillespie, 1976). We provide a brief mathematical summary of the model equations, whereas the other details, such as the detailed meaning and values of the parameters, can be found in Table S1 of the published supplementary materials (Song et al., 2012a). Parameter justifications, the relevant experimental measurements are discussed in the supplement materials (Song et al., 2012a).

In the Gillespie algorithm, the chemical system is assumed to be well-mixed for simplicity. The signalling pathway is decomposed into a set of unidirectional reactions, denoted as $R_u (u = 1, 2, \cdots, 12)$, each of which contains only unimolecular or bimolecular reactants (Table A1). In Table A1, the molecules, which are few, are counted; otherwise, concentrations are used. In general, X is the number of molecules; X* is the active state of X, and X_T the total number of corresponding molecules/channels inside a single microvillus. [X] is the concentration; $[X]_i$ is intracellular concentration, and $[X]_o$ the extracellular concentration.

Each of the reaction steps in Table A1 is characterised by a momentarily-defined stochastic reaction constant c_u, where $c_u \delta t$ denotes the average probability that a particular combination of R reactant molecules reacts accordingly in the next infinitesimal time interval δt. If h_u is the total number of R_u reactant pairs, then $a_u \delta t = c_u h_u \delta t$ is the average probability that reaction R_u will occur during δt. Assuming during δt, only 0 or 1 reaction occurs, dt (next reaction time increment) and R_u can be determined independently. When R_u is chosen, the state vector **X** is updated with a state transition vector, V_u. The procedure iterates until a termination criterion is satisfied; e.g. if the current simulation time, t, is larger than a preset value.

Table A1: The modelled reactions in the phototransduction cascade

Rection	Parameter	Parameter definition	Corresponding biological process
$M^* \xrightarrow{c_1} \emptyset$ (R1)	$c_1 = \gamma_{M^*}(1 + h_{M^*} f_n)$	κ and γ are the activation and deactivation rates, respectively	Inactivation of metarhodopsin (M*) by arrestin binding. $\emptyset$ indicates any product, whose kinetics are not modelled
$M^* + G \xrightarrow{c_2} M^* + G^*$ (R2)	$c_2 = \kappa_{G^*}$	f_p and f_n are the positive and feedbacks, respectively.	The activation of G into G* by M*. Three states are modelled, $G_\alpha G_{\beta\gamma}GDP$ (G), $G_\alpha GTP$ (G*) and $G_\alpha GTP$-PLC (PLC*)
$G^* + PLC \xrightarrow{c_3} PLC^*$ (R3)	$c_3 = \kappa_{PLC^*}$		G* binds to PLC and becomes an active G-protein-PLC complex (PLC*)

$G^* + PLC^*$ $\xrightarrow{c_4} G_\alpha GDP + PLC^*$ (R4)	$c_4 = \gamma_{GAP}$	$h_{*,p}$ and $h_{*,n}$ are the positive and negative feedback strength to the relevant molecular targets.	The conversion from $G_\alpha GTP$ to $G_\alpha GDP$ by GTPase activity of G*, catalysed by PLC*
$G_\alpha GDP \xrightarrow{c_5} G$ (R5)	$c_5 = \gamma_G$		$G_\alpha GTP$ then rebinds to $G_{\beta\gamma}$ before it can be reactivated
$PLC^* \xrightarrow{c_6} D^* + PLC^*$ (R6)	$c_6 = \gamma_{D^*}$	K_{D^*} is the transition rate from D* to the opening of TRP/TRPL.	PLC* hydrolyses PIP_2 into DAG and IP_3. Here, PLC* is modelled to activate the unknown excitation messenger D* directly
$PLC^* \xrightarrow{c_7} PLC + G_\alpha GDP$ (R7)	$c_7 = \gamma_{PLC^*}(1 + h_{PLC^*} f_n)$		PLC* decompose to PLC and $G_\alpha GDP$
$D^* \xrightarrow{c_8} \emptyset$ (R8)	$c_8 = \gamma_{D^*}(1 + h_{D^*} f_n)$	K_U and K_R are the uptake and release rate of Ca^{2+} from Calmodulin.	D* degrades
$2D^* + T \xrightarrow{c_9} T^*$ (R9)	$c_9 = \dfrac{\kappa_{T^*}(1 + h_{T^*,p} f_p)}{(K_{D^*})^2}$	V is the microvillus volume.	D* excites TRP/TRPL channels T to their open states (T^*)
$T^* \xrightarrow{c_{10}} T$ (R10)	$c_{10} = \gamma_{T^*}(1 + h_{T^*,n} f_n)$		open TRP/TRPL channels close
$Ca^{2+} + CaM \xrightarrow{c_{11}} C^*$ (R11)	$c_{11} = \dfrac{K_U}{V^2}$	The detailed meaning and values of the parameters can be found in Table S1 of supplementary materials of Song et al. in 2012.	Ca^{2+} binds to Calmodulin C^*
$C^* \xrightarrow{c_{12}} Ca^{2+} + CaM$ (R12)	$c_{12} = K_R$		the release of Ca^{2+} from Calmodulin

Assuming that, apart from Ca^{2+}, the molecular components cannot enter or leave the microvillus, the following mass balance equations hold in Table A2.

Table A2: Mass balance equations in the phototransduction cascade of a single microvillus

Mass balance equation	Definition	Number
$T^* + T = T_T$	The total amount of TRP/TRPL channels (T_T) is fixed	(1)
$CaM + C^* = C_T$	The total amount of Calmodulin (C_T) is fixed	(2)
$PLC^* + PLC = PLC_T$	The total amount of PLC (PLC_T) is fixed	(3)
$G^* GDP + G + G^* + PLC^* = G_T$	The total amount of G proteins (G_T) is fixed	(4)

Using these mass balance equations in Table A2, the number of state variables can be reduced, and the state vector, **X**, is defined as:

$$X = [M^*; G; G^*; PLC^*; D^*; C^*; T^*] \tag{5}$$

The state transition matrix, **V**, is defined as:

$$V = \begin{bmatrix} -1 & 0 & 0 & 0 & 0 & 0 & 0 & 0 & 0 & 0 & 0 & 0 \\ 0 & -1 & 0 & 0 & 1 & 0 & 0 & 0 & 0 & 0 & 0 & 0 \\ 0 & 1 & -1 & -1 & 0 & 0 & 0 & 0 & 0 & 0 & 0 & 0 \\ 0 & 0 & 1 & 0 & 0 & 0 & -1 & 0 & 0 & 0 & 0 & 0 \\ 0 & 0 & 0 & 0 & 0 & 1 & 0 & -1 & -2 & 0 & 0 & 0 \\ 0 & 0 & 0 & 0 & 0 & 0 & 0 & 0 & 0 & 0 & 1 & -1 \\ 0 & 0 & 0 & 0 & 0 & 0 & 0 & 0 & 1 & -1 & 0 & 0 \end{bmatrix} \qquad (6)$$

The number of reactant pairs for each reaction is:

$$h = \begin{array}{llll} [M^*; & M^*(G); & G^*(PLC_T - PLC^*); & G^*(PLC^*); \\ G_T - G^* - G - PLC^*; & PLC^*; & PLC^*; & D^*; \\ \frac{D^*(D^*-1)(T_T-T^*)}{2}; & T^*; & Ca^{2+}(CaM); & C^*] \end{array} \qquad (7)$$

With the definitions of **X, V, c, h,** the time increment dt, during which the next reaction R_u reacts, is determined by Eq.8, and R_u can be chosen so that Eq. 9 satisfies:

$$dt = \frac{1}{l_a + a_s} \ln\left(\frac{1}{r_1}\right) \qquad (8)$$

$$\sum_{v=1}^{u-1} a_v < r_2 a_s \leq \sum_{v=1}^{u} a_v \qquad (9)$$

where r_1 and r_2 are uniformly distributed random numbers. a_s is the dot product between c and h ($a_s = \sum_{u=1}^{M} c_u h_u$), and a_v is a product between c_v and h_v.

Ca dynamics: Ca^{2+} is an essential feedback signal in the phototransduction cascade. Ideally, Ca^{2+} should be included as one of the state variables, but because Ca^{2+} changes up to 1,000-fold during a bump, its dynamics are approximated by a deterministic approach to save computation time. The formulas to calculate Ca^{2+} and the relevant feedbacks are listed in Table 3. Ca^{2+} dynamics are assumed to be so fast that the stochastic simulation framework quantities are updated by the steady-state values.

Table 3: Formulas for Ca^{2+} dynamics in the microvillus

Formulas	Parameters	#
$\frac{d[Ca^{2+}]_i}{dt} = \frac{I_{Ca,net}}{2VF} - n\frac{d[C^*]_i}{dt} - K_{Ca}[Ca^{2+}]_i$	1st term: Ca^{2+} influx; 2nd term: Ca^{2+} uptake by calcium buffer; 3rd term: Ca2+ diffusion to the cell body; V: microvillus volume, F: Faraday constant. n: the number of Calmodulin Ca^{2+} binding sites. $1/K_{Ca}$ denotes Ca^{2+} diffusion time constant.	(10)
$I_{Ca,net} = I_{Ca} - 2I_{NaCa}$	I_{Ca}: Ca^{2+} influx through TRP/TRPL, calculated as 40% of total current influx; I_{NaCa}: Ca^{2+} extrusion from Na$^+$/Ca^{2+} exchanger	(11)
$I_{NaCa} = K_{NaCa}\left([Na^+]_i{}^3[Ca^{2+}]_o - [Na^+]_o{}^3[Ca^{2+}]_i e^{-\frac{V_m F}{RT}}\right)$	I_{NaCa} is calculated from a simplified Na$^+$/Ca^{2+} exchanger model, given that the extracellular ionic concentrations ae fixed and the cell is voltage-clamped; K_{NaCa}: scaling factor; V_m: the transmembrane potential; R: the gas constant; T: the absolute temperature	(12)
$\frac{d[C^*]_i}{dt} = K_u[Ca^{2+}]_i[CaM]_i - K_R[C^*]_i$	Dynamics of Ca^{2+} binding to CaM; K_U and K_R are the uptake and release rate of Ca^{2+} from Calmodulin.	(13)

$$f_p([Ca^{2+}]_i) = \frac{\left(\frac{[Ca^{2+}]_i}{K_P}\right)^{m_p}}{1+\left(\frac{[Ca^{2+}]_i}{K_P}\right)^{m_p}}$$

The positive and negative feedbacks are approximated by Hill functions of $[Ca^{2+}]_i$. (14)

K_p and K_n are the dissociation constants, i.e., the substances that provide half-occupancy of the binding sites; m_p and m_n are the Hill coefficients, describing the cooperativity of the excitation messengers

$$f_n([C^*]_i) = n_s * \frac{\left(\frac{[C^*]_i}{K_n}\right)^{m_n}}{1+\left(\frac{[C^*]_i}{K_n}\right)^{m_n}}$$

(15)

Despite the many model parameters, adaptation mechanisms can be regulated by only two mass parameters: n_s in Eq. 15 for the quantum bump (QB) shape and l_a in Eq. 8 to tune the width of the QB latency distribution. These parameters had little effect on the QB refractory period when the bump statistics were within the physiological range for *Drosophila* (Song et al., 2012).

Appendix D: Integration of Light-Induced Current (LIC)
The macroscopic light-induced current (LIC) of the rhabdomere is integrated from the current QBs of up to N_u microvilli. The formulas for the calculations are listed in Table 4:

Table 4: Formulas to calculate the macroscopic LIC

Formulas	Parameters	#
$I_{in}^N = I_{T^*} \times T^{*N}$	I_{in}^N is the (LIC) of microvillus N T^{*N}: the number of opened TRP/TRPL channels in microvillus N	(16)
$I_{T^*} = g_{TRP}(TRP_{rev} - V_m)$	I_{T^*} is the average single-channel current conducted by an open TRP/TRPL channel; g_{TRP} is the single TRP channel conductance TRP_{rev} is the TRP channel reversal potential; V_m is the photoreceptor membrane potential.	(17)
$g_{TRP} = 8 \times \begin{cases} 1 & if\ TRP_{rev} > V_m \\ 0 & otherwise \end{cases}$	Single-channel conductance is 8 pS, TRP_{rev} is 0 mV	(18)
$LIC = \sum_{N=1}^{N_u} I_{in}^N$	The microscopic LIC of the rhabdomere is integrated from the current QBs of up to N_u microvilli. From Eq. 17, as V_m increases, the bumps I_{in}^N shrink accordingly, LIC decreases. Thus, LIC and V_m are calculated iteratively.	(19)
$V_m = HH(LIC)$	V_m is obtained by injecting the macroscopic LIC in into the HH model of the cell body.	(20)

Appendix E: Hodgkin-Huxley Cell-Body Model
Appendix E describes the Hodgkin–Huxley model of the photoreceptor plasma membrane. This module transduces LIC into voltage response by reproducing the voltage-gated K+ conductance dynamics on the photon-insensitive membrane (Li et al., 2019; Niven et al., 2003). The model was adopted from (Niven et al., 2003); we only list the major equations and parameters. The details can be found in Vähäsöyrinki's PhD thesis (Vähäsöyrinki, 2004).

Table 5: Formulas for the HH model for the photoreceptor cell body

Formulas	Parameters		#
$$C_m \frac{dV_m}{dt} = LIC - \sum_i g_i(V_m - E_k) - g_L(V_m - E_L)$$ LIC is the macroscopic light-induced current integrated from all QBs in the rhabdomere. g_i represents various voltage-gated K$^+$ conductances, including fast inactivating *Shaker*, slow delayed rectifier, *Shab* conductances, and a slowly activating, non-inactivating voltage-gated K$^+$ conductance. g_L represents K$^+$ and Cl$^-$ leaks.	Resting potential	-66 mV	(21)
	Specific membrane capacitance	4 uF/cm²	
	Maximum *Shaker* conductance	0.8 mS/cm²	
	Maximum *Shab* conductance	3.0 mS/cm²	
	Maximum novel K$^+$ conductance	0.11 mS/cm²	
	Potassium leak conductance	0.0855 mS/cm²	
	Chloride leak conductance	0.0585 mS/cm²	
$$g_i = g_{imax} \prod_k [\gamma_k(V_m,t)]^n$$	g_{imax} represents the various maximum conductance listed above. n is the number of gating variables		(22)
$$\frac{d\gamma_k}{dt} = \alpha_\gamma(1 - \gamma_k) - \beta_\gamma \gamma_k$$			(23)
$$\alpha_k = \frac{[(g_\infty/g_{max})_k]^{1/n_k}}{\tau_k}$$	γ_k is the probability of the permissive state of the gating particles; α_γ and β_γ are voltage-dependent rate constants. Steady-state activation and inactivation curves		(24)
$$\beta_k = \frac{1 - [(g_\infty/g_{max})_k]^{1/n_k}}{\tau_k}$$	(g_∞) for voltage-gated K$^+$ channels were fitted to experimental data with Boltzmann function.		(25)
$$\left(\frac{g_\infty}{g_{max}}\right) = \frac{1}{1 + e^{\frac{V_{50}-V_m}{s}}}$$	V_{50} is the voltage producing a steady-state conductance of 50% of the maximum value, and s is the slope factor		(26)
$$\tau = \frac{1}{p_1 e^{\frac{p_2-V_m}{p_3}} + p_4 \frac{p_5 - V_m}{e^{\frac{p_5-V_m}{p_6}} - 1}}$$	The time constants of activation and inactivation curves were fitted to experimental data with a bell-shaped function, where p_i are the free parameters for fitting.		(27)

Table 5: Parameters for the HH model of the photoreceptor cell body

Variable	Shaker		Shab		Novel K$^+$
$V_{50}(mV)$	Act	Inact	Act	Inact	Act
	-23.7	1st -55.3 2nd -74.8	-1.0	-25.7	-14
$S(mV)$	12.8	1st -3.9 2nd -10.7	9.1	-6.4	10.6
n	3	1	2	1	1
τ p_1 p_2 p_3 p_4 p_5	0.008174 1.61882 24.6583 0.05813 -59.639	0.2303 -192.973 31.3196 0.04373 13.4859	0.1163 -25.6551 32.1933 0.006592 -23.8032	$\tau_{inact} = 1200\,ms$	$\tau_{acti} = (13 + \frac{6232}{30*\sqrt{\frac{\pi}{2}}}\exp(-2*(\frac{V_m+19.4}{30})^2)$

23

p_6	4.5012	11.11	1.3455

Author contributions

ZS conceptualised the paper; ZS & YZ wrote the first draft; MJ reshaped the draft and improved the figures, and MJ, ZS and JF edited the paper.

Conflict of interest statement

All authors declare no competing interests and gave final approval for publication.

Acknowledgements

References

Abbott LF, Lemasson G. Analysis of Neuron Models with Dynamically Regulated Conductances. Neural Computation, 1993; 5: 823-42.

Abou Tayoun AN, Li XF, Chu B, Hardie RC, Juusola M, Dolph PJ. The *Drosophila* SK Channel (dSK) Contributes to Photoreceptor Performance by Mediating Sensitivity Control at the First Visual Network. Journal of Neuroscience, 2011; 31: 13897-910.

Ahissar E, Arieli A. Seeing via miniature eye movements: a dynamic hypothesis for vision. Frontiers in Computational Neuroscience, 2012; 6.

Bhalla US. Molecular computation in neurons: a modeling perspective. Curr Opin Neurobiol, 2014; 25: 31-7.

Bhalla US. Multiscale interactions between chemical and electric signaling in LTP induction, LTP reversal and dendritic excitability. Neural Networks, 2011; 24: 943-9.

Bhalla US, Iyengar R. Emergent properties of networks of biological signaling pathways. Science, 1999; 283: 381-7.

Carrera J, Covert MW. Why Build Whole-Cell Models? Trends in Cell Biology, 2015; 25: 719-22.

Clark DA, Benichou R, Meister M, da Silveira RA. Dynamical Adaptation in Photoreceptors. Plos Comput Biol, 2013; 9.

Dau A, Friederich U, Dongre S, Li XF, Bollepalli MK, Hardie RC, Juusola M. Evidence for Dynamic Network Regulation of *Drosophila* Photoreceptor Function from Mutants Lacking the Neurotransmitter Histamine. Frontiers in Neural Circuits, 2016; 10.

De Schutter E. Why are computational neuroscience and systems biology so separate? Plos Comput Biol, 2008; 4.

Ditchburn RW, Ginsborg BL. Vision with a Stabilized Retinal Image. Nature, 1952; 170: 36-7.

Faivre O, Juusola M. Visual Coding in Locust Photoreceptors. Plos One, 2008; 3.

Franklin J, Bair W. The Effect of a Refractory Period on the Power Spectrum of Neuronal Discharge. Siam Journal on Applied Mathematics, 1995; 55: 1074-93.

French AS, Korenberg MJ, Järvilehto M, Kouvalainen E, Juusola M, Weckström M. The Dynamic Nonlinear Behavior of Fly Photoreceptors Evoked by a Wide-Range of Light Intensities. Biophysical Journal, 1993; 65: 832-9.

Friederich U, Billings SA, Hardie RC, Juusola M, Coca D. Fly Photoreceptors Encode Phase Congruency. Plos One, 2016; 11.

Friederich U, Coca D, Billings S, Juusola M. Data Modelling for Analysis of Adaptive Changes in Fly Photoreceptors. Neural Information Processing, Pt 1, Proceedings, 2009; 5863: 34-+.

Geurten BRH, Jahde P, Corthals K, Gopfert MC. Saccadic body turns in walking Drosophila. Frontiers in Behavioral Neuroscience, 2014; 8.

Gillespie DT. General Method for Numerically Simulating Stochastic Time Evolution of Coupled Chemical-Reactions. Journal of Computational Physics, 1976; 22: 403-34.

Goldberg AP, Szigeti B, Chew YH, Sekar JAP, Roth YD, Karr JR. Emerging whole-cell modeling principles and methods. Current Opinion in Biotechnology, 2018; 51: 97-102.

Gonzalez-Bellido PT, Wardill TJ, Juusola M. Compound eyes and retinal information processing in miniature *dipteran* species match their specific ecological demands. Proceedings of the National Academy of Sciences of the United States of America, 2011; 108: 4224-9.

Goriounova NA, Heyer DB, Wilbers R, Verhoog MB, Giugliano M, Verbist C, Obermayer J, Kerkhofs A, Smeding H, Verberne M, Idema S, Baayen JC, Pieneman AW, de Kock CPJ, Klein M, Mansvelder HD. Large and fast human pyramidal neurons associate with intelligence. Elife, 2018; 7.

Hardie RC. Whole-Cell Recordings of the Light-Induced Current in Dissociated *Drosophila* Photoreceptors - Evidence for Feedback by Calcium Permeating the Light-Sensitive Channels. Proceedings of the Royal Society B-Biological Sciences, 1991; 245: 203-10.

Hardie RC, Juusola M. Phototransduction in *Drosophila*. Curr Opin Neurobiol, 2015; 34: 37-45.

Hardie RC, Minke B. The Trp Gene Is Essential for a Light-Activated Ca2+ Channel in *Drosophila* Photoreceptors. Neuron, 1992; 8: 643-51.

Hardie RC, Peretz A, Susstoby E, Romglas A, Bishop SA, Selinger Z, Minke B. Protein-Kinase-C Is Required for Light Adaptation in *Drosophila* Photoreceptors. Nature, 1993; 363: 634-7.

Hardie RC. TRP channels and lipids: from Drosophila to mammalian physiology. J Physiol, 2007; 578: 9-24.

Hardie RC, Postma M. Phototransduction in microvillar photoreceptors of *Drosophila* and other invertebrates. In Masland RH, Albright TD, editors. The Senses: A Comprehensive Reference. Elsevier, 2008: 77-130.

Hardie RC, Raghu P, Moore S, Juusola M, Baines RA, Sweeney ST. Calcium influx via TRP channels is required to maintain PIP2 levels in *Drosophila* photoreceptors. Neuron, 2001; 30: 149-59.

Heeger DJ. Normalisation of Cell Responses in Cat Striate Cortex. Visual Neuroscience, 1992; 9: 181-97.

Hemberger M, Pammer L, Laurent G. Comparative approaches to cortical microcircuits. Curr Opin Neurobiol, 2016; 41: 24-30.

Henderson SR, Reuss H, Hardie RC. Single photon responses in *Drosophila* photoreceptors and their regulation by Ca^{2+}. Journal of Physiology-London, 2000; 524: 179-94.

Herz AVM, Gollisch T, Machens CK, Jaeger D. Modeling single-neuron dynamics and computations: A balance of detail and abstraction. Science, 2006; 314: 80-5.

Hochstrate P, Hamdorf K. Microvillar Components of Light Adaptation in Blowflies. Journal of General Physiology, 1990; 95: 891-910.

Hodgkin AL, Huxley AF. A Quantitative Description of Membrane Current and Its Application to Conduction and Excitation in Nerve. Journal of Physiology-London, 1952; 117: 500-44.

Howard J, Blakeslee B, Laughlin SB. The Intracellular Pupil Mechanism and Photoreceptor Signal - Noise Ratios in the Fly Lucilia-Cuprina. Proceedings of the Royal Society Series B-Biological Sciences, 1987; 231: 415-35.

Izhikevich EM. Which model to use for cortical spiking neurons? IEEE Trans Neural Netw. 2004 Sep;15:1063-70. doi: 10.1109/TNN.2004.832719.

Juusola M, Dau A, Song Z, Solanki N, Rien D, Jaciuch D, Dongre S, Blanchard F, de Polavieja GG, Hardie RC, Takalo J. Microsaccadic sampling of moving image information provides *Drosophila* hyperacute vision. Elife, 2017; 6.

Juusola M, Dau A, Zheng L, Rien DN. Electrophysiological Method for Recording Intracellular Voltage Responses of *Drosophila* Photoreceptors and Interneurons to Light Stimuli *In Vivo*. Jove-Journal of Visualized Experiments, 2016.

Juusola M, de Polavieja GG. The rate of information transfer of naturalistic stimulation by graded potentials. Journal of General Physiology, 2003; 122: 191-206.

Juusola M, French AS. The efficiency of sensory information coding by mechanoreceptor neurons. Neuron, 1997; 18: 959-68.

Juusola M, French AS, Uusitalo RO, Weckström M. Information processing by graded-potential transmission through tonically active synapses. Trends in Neurosciences, 1996; 19: 292-7.

Juusola M, Hardie RC. Light adaptation in *Drosophila* photoreceptors: I. Response dynamics and signaling efficiency at 25 degrees C. Journal of General Physiology, 2001a; 117: 3-25.

Juusola M, Hardie RC. Light adaptation in *Drosophila* photoreceptors: II. Rising temperature increases the bandwidth of reliable signaling. Journal of General Physiology, 2001b; 117: 27-41.

Juusola M, Kouvalainen E, Jarvilehto M, Weckstrom M. Contrast Gain, Signal-to-Noise Ratio, and Linearity in Light-Adapted Blowfly Photoreceptors. Journal of General Physiology, 1994; 104: 593-621.

Juusola M, Song Z. How a fly photoreceptor samples light information in time. Journal of Physiology-London, 2017; 595: 5427-37.

Juusola M, Song Z, Hardie R. Phototransduction biophysics. In Jaeger D, Jung R, editors. Encyclopedia of Computational Neuroscience. Springer: New York, 2015: 2359-76.

Juusola M, Uusitalo RO, Weckström M. Transfer of Graded Potentials at the Photoreceptor Interneuron Synapse. Journal of General Physiology, 1995a; 105: 117-48.

Juusola M, Weckström M, Uusitalo RO, Korenberg MJ, French AS. Nonlinear models of the first synapse in the light-adapted fly retina. Journal of Neurophysiology, 1995b; 74: 2538-47.

Kim B, Hawes SL, Gillani F, Wallace LJ, Blackwell KT. Signaling Pathways Involved in Striatal Synaptic Plasticity are Sensitive to Temporal Pattern and Exhibit Spatial Specificity. Plos Comput Biol, 2013; 9.

Klipp E, Liebermeister W. Mathematical modeling of intracellular signaling pathways. Bmc Neurosci, 2006; 7.

Kotter R, Schirok D. Towards an integration of biochemical and biophysical models of neuronal information processing: A case study in the nigro-striatal system. Rev Neuroscience, 1999; 10: 247-66.

Land BR, Salpeter EE, Salpeter MM. Kinetic-Parameters for Acetylcholine Interaction in Intact Neuromuscular-Junction. P Natl Acad Sci-Biol, 1981; 78: 7200-4.

Laughlin SB, Lillywhite PG. Intrinsic Noise in Locust Photoreceptors. Journal of Physiology-London, 1982; 332: 25-45.

Li XF, Abou Tayoun A, Song ZY, Dau A, Rien D, Jaciuch D, Dongre S, Blanchard F, Nikolaev A, Zheng L, Bollepalli MK, Chu B, Hardie RC, Dolph PJ, Juusola M. Ca^{2+}-Activated K^+ Channels Reduce Network Excitability, Improving Adaptability and Energetics for Transmitting and Perceiving Sensory Information. Journal of Neuroscience, 2019; 39: 7132-54.

Lillywhite PG. Single-Photon Signals and Intrinsic Noise in Locust Photoreceptors. Journal of the Optical Society of America, 1979; 69: 1469-.

Lillywhite PG, Laughlin SB. Transducer Noise in a Photoreceptor. Nature, 1979; 277: 569-72.

Marder E, Goaillard JM. Variability, compensation and homeostasis in neuron and network function. Nat Rev Neurosci, 2006; 7: 563-74.

Markram H. The Blue Brain Project. Nat Rev Neurosci, 2006; 7: 153-60.

Markram H. The human brain project. Sci Am, 2012; 306: 50-5.

Markram H, Muller E, Ramaswamy S, Reimann MW, Abdellah M, Sanchez CA, Ailamaki A, Alonso-Nanclares L, Antille N, Arsever S, Kahou GAA, Berger TK, Bilgili A, Buncic N, Chalimourda A, Chindemi G, Courcol JD, Delalondre F, Delattre V, Druckmann S, Dumusc R, Dynes J, Eilemann S, Gal E, Gevaert ME, Ghobril JP, Gidon A, Graham JW, Gupta A, Haenel V, Hay E, Heinis T, Hernando JB, Hines M, Kanari L, Keller D, Kenyon J, Khazen G, Kim Y, King JG, Kisvarday Z, Kumbhar P, Lasserre S, Le Be JV, Magalhaes BRC, Merchan-Perez A, Meystre J, Morrice BR, Muller J, Munoz-Cespedes A, Muralidhar S, Muthurasa K, Nachbaur D, Newton TH, Nolte M, Ovcharenko A, Palacios J, Pastor L, Perin R, Ranjan R, Riachi I, Rodriguez JR, Riquelme JL, Rossert C, Sfyrakis K, Shi Y, Shillcock JC, Silberberg G, Silva R, Tauheed F, Telefont M, Toledo-Rodriguez M, Trankler T, Van Geit W, Diaz JV, Walker R, Wang Y, Zaninetta SM, DeFelipe J, Hill SL, Segev I, Schurmann F. Reconstruction and Simulation of Neocortical Microcircuitry. Cell, 2015; 163: 456-92.

Marr D. Vision: A Computational Investigation into the Human Representation and Processing of Visual Information. The MIT Press, 1982.

Mayer J, Khairy K, Howard J. Drawing an elephant with four complex parameters. American Journal of Physics, 2010; 78: 648-9.

Meinertzhagen IA, O'Neil SD. Synaptic organisation of columnar elements in the lamina of the wild type in *Drosophila melanogaster*. J Comp Neurol, 1991; 305: 232-63.

Naoki H, Sakumura Y, Ishii S. Local signaling with molecular diffusion as a decoder of Ca2+ signals in synaptic plasticity. Mol Syst Biol, 2005; 1.

Niven JE, Vahasoyrinki M, Kauranen M, Hardie RC, Juusola M, Weckstrom M. The contribution of Shaker K$^+$ channels to the information capacity of *Drosophila* photoreceptors. Nature, 2003; 421: 630-4.

Ostojic S, Brunel N. From Spiking Neuron Models to Linear-Nonlinear Models. Plos Comput Biol, 2011; 7.

Packer O, Williams DR. Blurring by Fixational Eye-Movements. Vision Res, 1992; 32: 1931-9.

Poo MM, Du JL, Ip NY, Xiong ZQ, Xu B, Tan T. China Brain Project: Basic Neuroscience, Brain Diseases, and Brain-Inspired Computing. Neuron, 2016; 92: 591-6.

Pumir A, Graves J, Ranganathan R, Shraiman BI. Systems analysis of the single photon response in invertebrate photoreceptors. Proceedings of the National Academy of Sciences of the United States of America, 2008; 105: 10354-9.

Rabinovich M, Huerta R, Laurent G. Neuroscience - Transient dynamics for neural processing. Science, 2008; 321: 48-50.

Rall W. Branching Dendritic Trees and Motoneuron Membrane Resistivity. Exp Neurol, 1959; 1: 491-527.

Rall W. Theoretical significance of dendritic trees for neuronal input-output relations. In Reiss RF, editor. Neural Theory and Modeling. Stanford University Press, 1964.

Ratliff CP, Borghuis BG, Kao YH, Sterling P, Balasubramanian V. Retina is structured to process an excess of darkness in natural scenes. Proceedings of the National Academy of Sciences of the United States of America, 2010; 107: 17368-73.

Rieke F, Bodnar DA, Bialek W. Naturalistic stimuli increase the rate and efficiency of information transmission by primary auditory afferents. Proceedings of the Royal Society B-Biological Sciences, 1995; 262: 259-65.

Rieke F, Rudd ME. The Challenges Natural Images Pose for Visual Adaptation. Neuron, 2009; 64: 605-16.

Rivera-Alba M, Vitaladevuni SN, Mishchenko Y, Lu Z, Takemura SY, Scheffer L, Meinertzhagen IA, Chklovskii DB, de Polavieja GG. Wiring economy and volume exclusion determine neuronal placement in the *Drosophila* brain. Curr Biol, 2011; 21: 2000-5.

Shannon CE. A Mathematical Theory of Communication. Bell System Technical Journal, 1948; 27: 379-423.

Silva GA, Hetling JR, Pepperberg DR. Dynamic and steady-state light adaptation of mouse rod photoreceptors in vivo. Journal of Physiology-London, 2001; 534: 203-16.

Smolen P, Baxter DA, Byrne JH. Molecular Constraints on Synaptic Tagging and Maintenance of Long-Term Potentiation: A Predictive Model. Plos Comput Biol, 2012; 8.

Song Z, Banks RW, Bewick GS. Modelling the mechanoreceptor's dynamic behaviour. Journal of Anatomy, 2015; 227: 243-54.

Song Z, Coca D, Billings S, Postma M, Hardie RC, Juusola M. Biophysical modeling of a *Drosophila* photoreceptor. Neural Information Processing, Pt 1, Proceedings 2009: 57-71.

Song Z, Juusola M. A biomimetic fly photoreceptor model elucidates how stochastic adaptive quantal sampling provides a large dynamic range. Journal of Physiology-London, 2017; 595: 5439-56.

Song Z, Juusola M. Refractory Sampling Links Efficiency and Costs of Sensory Encoding to Stimulus Statistics. Journal of Neuroscience, 2014; 34: 7216-37.

Song Z, Postma M, Billings SA, Coca D, Hardie RC, Juusola M. Stochastic, Adaptive Sampling of Information by Microvilli in Fly Photoreceptors. Current Biology, 2012a; 22: 1371-80.

Song Z, Postma M, Billings SA, Coca D, Hardie RC, Juusola M. Stochastic, adaptive sampling of information by microvilli in fly photoreceptors. Curr Biol, 2012b; 22: 1371-80.

Song Z, Zhou Y, Juusola M. Modeling elucidates how refractory period can provide profound nonlinear gain control to graded potential neurons. Physiological Reports, 2017; 5.

Song Z, Zhou Y, Juusola M. Random Photon Absorption Model Elucidates How Early Gain Control in Fly Photoreceptors Arises from Quantal Sampling. Frontiers in Computational Neuroscience, 2016; 10.

Stiles JR, Bartol TM. Monte Carlo methods for simulating realistic synaptic microphysiology using MCell. In

Szalavitz M. Brain Map: President Obama Proposes First Detailed Guide of Human Brain Function. Time. February 19, 2013.

De Schutter E, editor. Computational neuroscience: realistic modeling for experimentalists. CRC Press:: Bota Racon, Florida, 2000: 87-127.

Vähäsöyrinki M. Voltage-gated K+ Channels in Drosophila photoreceptors. Department of Physical Sciences, Division of Biophysics. University of Oulu, Finland, 2004.

Vähäsöyrinki M, Niven JE, Hardie RC, Weckström M, Juusola M. Robustness of neural coding in *Drosophila* photoreceptors in the absence of slow delayed rectifier K$^+$ channels. Journal of Neuroscience, 2006; 26: 2652-60.

van der Schaaf A, van Hateren JH. Modelling the power spectra of natural images: Statistics and information. Vision Res, 1996; 36: 2759-70.

van Hateren JH. Processing of natural time series of intensities in the early visual system of the blowfly. Perception, 1997; 26: 6-7.

van Hateren JH, Snippe HP. Phototransduction in primate cones and blowfly photoreceptors: different mechanisms, different algorithms, similar response. Journal of Comparative Physiology a-Neuroethology Sensory Neural and Behavioral Physiology, 2006; 192: 187-97.

van Kleef JP, Stange G, Ibbotson MR. Applicability of White-Noise Techniques to Analyzing Motion Responses. Journal of Neurophysiology, 2010; 103: 2642-51.

van Vreeswijk, C., and H. Sompolinsky. 1998. Chaotic balanced state in a model of cortical circuits. Neural Comput, 10: 1321-71.

Vayttaden SJ, Ajay SM, Bhalla US. A spectrum of models of signaling pathways. Chembiochem, 2004; 5: 1365-74.

Wardill TJ, List O, Li XF, Dongre S, McCulloch M, Ting CY, O'Kane CJ, Tang SM, Lee CH, Hardie RC, Juusola M. Multiple Spectral Inputs Improve Motion Discrimination in the Drosophila Visual System. Science, 2012; 336: 925-31.

Wark B, Lundstrom BN, Fairhall A. Sensory adaptation. Curr Opin Neurobiol, 2007; 17: 423-9.

Wong F, Knight BW. Adapting-Bump Model for Eccentric Cells of *Limulus*. Journal of General Physiology, 1980; 76: 539-57.

Wong F, Knight BW, Dodge FA. Adapting Bump Model for Ventral Photoreceptors of *Limulus*. Journal of General Physiology, 1982; 79: 1089-113.

Wong F, Knight BW, Dodge FA. Dispersion of Latencies in Photoreceptors of *Limulus* and the Adapting-Bump Model. Journal of General Physiology, 1980; 76: 517-37.

Zheng L, de Polavieja GG, Wolfram V, Asyali MH, Hardie RC, Juusola M. Feedback network controls photoreceptor output at the layer of first visual synapses in *Drosophila*. Journal of General Physiology, 2006; 127: 495-510.

Zheng L, Nikolaev A, Wardill TJ, O'Kane CJ, de Polavieja GG, Juusola M. Network Adaptation Improves Temporal Representation of Naturalistic Stimuli in *Drosophila* Eye: I Dynamics. Plos One, 2009; 4.